

**This article is published in**

**Palaeogeography, Palaeoclimatology, Palaeoecology(2009)**

**volume 278, 71-87**

**doi:10.1016/j.palaeo.2009.03.019**

# **Loess-like and palaeosol sediments from Lanzarote (Canary Islands/Spain) — Indicators of palaeoenvironmental change during the Late Quaternary**

Suchodoletz, H. von<sup>a\*</sup>, Kühn, P.<sup>b</sup>, Hambach, U.<sup>a</sup>, Dietze, M.<sup>c</sup>, Zöller, L.<sup>a</sup> & D. Faust<sup>c</sup>

<sup>a</sup> Department of Geomorphology, University of Bayreuth, Germany

<sup>b</sup> Institute of Geography, Chair of Physical Geography, Eberhard Karls University of Tübingen, Germany

<sup>c</sup> Institute of Geography, Technical University of Dresden, Germany

\* *Hans.vonSuchodoletz@uni-bayreuth.de*

## ***abstract:***

On Lanzarote (Canary Islands) Quaternary Saharan dust and weathered local volcanic material were trapped in Miocene to Pliocene valleys dammed by younger volcanic edifices. These sediments show sequences of alternating reddish/clayey and loess-like yellowish/silty material. In order to investigate if reddish/clayey layers contain material derived from local pedogenesis and if so, which pedogenetic processes were active, we performed sedimentological, micromorphological and environmental magnetic analyses. The analyses demonstrate that these layers contain material derived from local soils. These soils were characterised by clay formation, rubefication and the formation of superparamagnetic particles during periods of enhanced soil moisture. Thus, they can serve as natural archives in order to reconstruct the terrestrial palaeoclimatic history of Lanzarote. The distribution of soil material in the profiles shows that cold periods of the Late Quaternary were characterised by more humid conditions than today. Using palaeontological remains and a comparison with recent soils on Tenerife, we can roughly estimate maximal palaeoprecipitation values during more humid periods.

## **1. Introduction**

Loess-palaeosol sequences are important terrestrial palaeoclimate archives for the past few million years as documented by numerous multiproxy-studies from both hemispheres (e.g. Bronger, 1976; Maher and Thompson, 1992; Dodonov and Baiguzina, 1995; Antoine et al. 2001; Schellenberger and Veit, 2006). In these sediments, palaeosol horizons are formed by various pedogenetic processes such as clay formation, rubefication or humus accumulation

and indicate enhanced soil moisture compared to periods when unweathered loess was deposited. Enhanced soil moisture indicates a more positive landscape water budget and is therefore connected to more humid climate conditions (e.g. Bush et al., 2004; Carter-Stiglitz et al., 2006). Pedogenetic processes and thus the intensity of pedogenesis in such sequences can be traced back using variations of several proxies, e.g. clay content, clay mineral assemblages, carbonate contents, isotopic composition of organic matter and soil carbonates, micromorphological features or environmental magnetic parameters (e.g. Bronger and Heinkele, 1989; Heinkele, 1990; Junfeng et al., 1999; Hatté et al., 2001; Maher et al., 2002; Markovic et al., 2008).

Enviromagnetism, the magnetism of sediments and soils, describes the occurrence, abundance and properties of iron-bearing minerals in the environment. Magnetic grains, exclusively iron oxides/hydroxides and sulphides, occur virtually ubiquitously in Quaternary sediments, soils, dust and organisms, albeit often in minor or trace concentrations. After sedimentation and/or reworking, they undergo diagenesis and pedogenesis when, for example, more humid conditions predominate. This can result in their transformation, depletion, neo-formation or enhancement. Ferrimagnetic minerals in particular react several orders of magnitude more strongly in ambient laboratory magnetic fields than other iron-bearing minerals. These minerals control the magnetic properties of sediments or soils even when present in very small amounts. Since climate changes and human activity produce changes in sedimentary and soil-forming environments, magnetic properties from a wide range of marine and continental sedimentary archives reflect alternating warm/humid and cold/dry climates during the Quaternary (e.g. Walden et al., 1999; Hambach et al., 2008).

The properties of a magnetic assemblage depend not merely on the composition of the minerals, but largely on the grain size distribution of the particles. For a given mineral, initial magnetic susceptibility ( $\kappa$ ) varies over orders of magnitude depending only on grain size.  $\kappa$  is largest for very fine superparamagnetic (SP) particles (roughly  $<30$  nm), is reduced for single domain (SD) grains and increases again for multi domain grains (roughly  $>140$  nm, valid for magnetite), although not reaching the values of superparamagnetic particles (e.g. Evans and Heller, 2003). Nowadays, essentially three models of the origin of ultrafine superparamagnetic minerals are discussed. (i) Firstly, large magnetic mineral grains may be decomposed or even “split” into smaller grains by weathering processes, producing large amounts of superparamagnetic particles when a relatively high concentration of magnetic minerals is present (Maher, 1998; van Velzen and Dekkers, 1999). (ii) Secondly, bacteria produce extracellular superparamagnetic Fe-minerals in different sedimentary or soil

environments, a process obviously omnipresent in soils (Maher, 1998). Fassbinder et al. (1990) first demonstrated the occurrence of so-called magnetotactic bacteria in soils. These bacteria produce intracellular low susceptible, but highly magnetic particles in the single domain state as means of spatial orientation, thereby causing magnetic enhancement as observed in non-volcanic soils. (iii) Thirdly, recent works of Torrent et al. (2006) and Liu et al. (2008) demonstrate the importance of the ferrihydrite → hydromaghemite → hematite transformation.

This transformation may constitute a major pathway accounting for the magnetic enhancement in many soils. The production of superparamagnetic hydromaghemite particles concurrently increases both the initial and frequency dependent magnetic susceptibility.

The Saharan desert is the largest source of dust in the world, contributing about 50% of all mobilised mineral aerosols (Aléon et al., 2002). This dust accumulates in the circum-Saharan area and is called “warm” or “desert” loess, in contrast to lithologically similar deposits in boreal and temperate zones derived from material mobilised by periglacial processes (e.g. Yaalon and Bruins, 1977; Coudé-Gaussen, 1991; Wright, 2001; Dearing et al., 2001).

About 30–50% of the dust originating from the Saharan desert is transported to the Atlantic Ocean (Goudie and Middleton, 2001; Prospero and Lamb, 2003). The Canary Islands are located at the northern fringe of this Atlantic Saharan dust plume, and aerosol deposition is well documented since the Middle Pleistocene (Moreno et al., 2001; Bozzano et al., 2002). On Lanzarote, Saharan dust and volcanic material are trapped in valleys which have developed in Miocene to Pliocene volcanic massifs and were at least partly dammed by younger volcanic material during the Early to Middle Pleistocene (Instituto Tecnológico y Geominero de España, 2005; Zöller et al., 2006). The trapped sediments show alternating distinct beds of reddish/clayey and loess-like yellowish/silty material. Previous soil studies in Lanzarote mainly focussed on slope sediments (Jahn, 1988; Schüle et al., 1989; Zarei, 1989), whereas the sequences developed in valley positions and exposed in profiles up to 7 m thickness (Zöller et al., 2003) have not yet been the focus of pedostratigraphical investigations. Recent geomorphological investigations revealed that a part of these valley sediments were directly deposited as aeolian fallout, whereas the larger part was colluvially reworked from the slopes. Both types of sediment alternate frequently (high frequency/low magnitude) and are partly mixed by vertic peloturbation processes, thus appearing as homogenous layers today (von Suchodoletz et al., 2009). The fact that erosion occurred with high frequency and low magnitude is demonstrated by a recent (and as demonstrated in this paper, past-) precipitation regime causing high landscape instability (cf. Langbein and Schumm, 1958). It is further

demonstrated by the largely continuous sedimentation rate found in the valley base. This is revealed by luminescence datings, yielding sediment ages ranging from Holocene to Mid-Pleistocene ( $>180$  ka)(Zöller et al., 2003; von Suchodoletz et al., 2008).

We propose that the alternation of loess-like yellowish/silty and reddish/clayey layers reflects differing periods of weathering on the island, regardless of the geomorphic position of the material (slope, valley) during weathering. Therefore, these sequences should reflect climatic changes, where properties such as reddish color and high clay content developed during more humid periods (Zöller et al., 2003; von Suchodoletz et al., 2009).

In this paper, we apply various sedimentological and pedological methods such as investigations of clay content, environmental magnetic parameters (measurement of initial and frequency dependent magnetic susceptibility as well as remanence properties), clay mineral composition and micromorphological features, in order to understand pedogenetic properties and processes. Based on this understanding, we are able to attempt a reconstruction of palaeoenvironmental conditions.

## **2. Geographic setting**

Lanzarote is the northeasternmost of the volcanic Canary islands, and is situated 130 km off the coast of NW Africa between  $28^{\circ}50'$  to  $29^{\circ}13'N$  and  $13^{\circ}25'$  to  $13^{\circ}52'W$  (Fig. 1).

Volcanism started during the Miocene about 15.5 Ma ago and lasted until recent (1730–36 last volcanic eruptions) (e.g. Carracedo et al., 1998). Both the northern and the southern parts of the island are dominated by Miocene to Pliocene volcanic massifs. Volcanism is basic, forming basalts and pyroclastics (cf. Rothe, 1996). Consequently, Jahn (1988) and Mizota and Matsuhisa (1995) demonstrate that all quartz found on the island must have an allochthonous origin.

Due to strong erosion, the relief of Lanzarote is generally smooth with concave slopes. The maximal altitude of the island is only 670 m. Several phases of soil forming processes resulted in the formation of polygenetic calcretes exposed along the slopes through erosion. The volcanic complexes in the north and the south of the island are separated by a central part exhibiting a smoother topography, and they are further dissected by numerous U-shaped valleys and smaller gullies. Some of the larger valleys were dammed by volcanic material (lava flows, pyroclastica) during the Early and Middle Pleistocene and thus served as sediment traps for Saharan dust and local volcanic material. On Lanzarote, these dammed valleys are called vegas. The climate of Lanzarote is maritime-semiarid. Due to the limited

elevation of the island, Lanzarote gets no precipitation from orographically raising trade wind air. Thus, it receives only very sparse precipitation from boreal winter cyclones, ranging from 100 to 250 mm/a and decreasing from higher to lower altitudes. Mean annual temperature at sea level is  $19.9 \pm 3$  °C (Jahn, 1988). The vegetation is very sparse, shrubby and disperse, dominated by xerophytic and halophytic species. The vegetation cover is mainly controlled by anthropogenic activity (Jahn, 1988; Kunkel, 1993).

Saharan dust is brought to the island mainly during two different synoptic situations: During winter, Calima events advect dust at low latitude (0–1500 m) to the archipelago. Calima-winds are continental African Tradewinds (Harmattan) deflected towards the west by Atlantic cyclones situated close to the Canary Islands (cf. Criado and Dorta, 2003). During summer, dust is transported to latitudes north of the Canary Islands by the northern branch of the Saharan Air Layer which is active within an altitude of about 1500 to 5500 m a.s.l. There, the material advects into the lowermost troposphere and is finally transported towards the island by the Northeast Trade wind (cf. Koopmann, 1981; Bozzano et al., 2002). Finally, dust sedimentation is either by dry or wet deposition (Criado and Dorta, 2003; Menéndez et al., 2007).

### **3. Studied sites**

Three vegas in the north and the south of Lanzarote were investigated (Fig. 1, Table 1). The valley slopes underwent long-term alteration through several soil forming periods, as evidenced by polygenetic calcretes, and thus have a flat shape. The profiles investigated are taken from sites remote from geomorphic active slopes. The sediments consist of a mixture of in situ and reworked fluvioaeolian material, derived from both allochthonous Saharan dust and from autochthonous volcanic material. High quartz contents in the sediments (Jahn, 1988; Zöller et al., 2004) indicate that Saharan dust is the main contributor. The sequences are characterised by a change of reddish/clayey and loess-like, yellowish/silty layers. Several layers exhibit carbonate nodules as well as calcified root channels and vertical cracks, in some cases hardened to calcrete horizons. Loess-like layers in particular show ferromanganese concretions up to 2 cm in diameter or calcified nests of ground-nesting anthophora bees (Fig. 2). The upper parts of the sequences are characterised by anthropogenically influenced colluvial deposits of varying thickness, some containing ovicaprid bones (Zöller et al., 2003; von Suchodoletz et al., 2009). Details of the studied sites are listed in Table 1.

### **4. Methods**

Grain size analyses were performed in two different ways:

- (1) For relative analyses, sediment samples were collected in an equidistant interval of 5 cm. 10 g of sediment were treated with 10 and 30% HCl at 65 °C to remove carbonate and dolomite. Subsequently, organic carbon was destroyed using 32% H<sub>2</sub>O<sub>2</sub>. Sand was removed by wet sieving, and the fraction >63 µm was treated for some hours in an ultrasonic bath to disintegrate abundant aggregates containing clay and ferromanganese oxides and -hydroxides which would strongly bias the grain size results (Fig. 3). After adding 0.1 M sodium pyrophosphate and subsequent shaking for 24 h in order to disperse clay particles, the samples were measured using a Malvern 2600C Analyser at GFZ Potsdam/Germany. For interpretation, the mean of three successive measurements recording 32 grain size classes was taken. Following Konert and Vandenberghe (1997), we used a conspicuous inflection point of the grain size distributions separating the first dominant peak from the following, thus obtaining a limit clay/silt of 6.18 µm. In order to get the weathering signal, the ratio of clay and the fraction >42 µm was taken to remove the signal of coarse silt. Coarse silt and fine sand show very similar depth functions, and due to their smaller specific surface they are believed not to contribute to weathering on the island as strongly as fine/middle silt (cf. Helgeson et al., 1984).
- (2) Absolute clay contents from selected layers in Femés were determined using pipette analyses (cf. Konert and Vandenberghe, 1997). A suspension of 20 g pretreated and sieved sample material >63 µm and of 1 l deionized water was filled into a Koehn-cylinder and shaken. Aliquots of clay, fine, middle and coarse silt were taken from the suspension at time intervals determined by Stoke's law. Obtained aliquots were dried and weighed and related to the original sample weight.

Environmental magnetic analyses were carried out on bulk samples taken in a distance of 5 cm. The dried sediment was packed into plastic boxes, and subsequently compressed and fixed with cotton wool in order to prevent movement of sediment particles during measurement before closing the lid. The sediment mass served as a normalizer. Because the original in situ sediment density and the exact volume of the boxes were unknown we assumed an average density of  $1.7 \cdot 10^3 \text{ kg m}^{-3}$  in order to calculate volume susceptibility ( $\kappa$ ). The initial low field susceptibility was measured in an AC-field of 300 A/m at 920 Hz using the KLY-3-Spinner-Kappa-Bridge (AGICO, Brno, Czech Republic). The frequency dependence of susceptibility ( $\kappa_{fd}$ ) was determined with a MAGNON Susceptibility Bridge (MAGNON, Dassel, Germany) at AC-fields of 80 A/m at 1 and 8 kHz respectively  $\kappa_{fd} = (\kappa @ 1$

kHz $\rightarrow$ κ@8 kHz)/κ@1 kHz\*100 in %). In order to investigate the remanence properties we exposed the samples to pulse-fields of 2 T and 0.35 T (antiparallel), respectively, using a Magnon PM II pulse magnetizer (MAGNON; Dassel, Germany). Acquired remanence (isothermal remanent magnetization, IRM@2T) was subsequently measured with a JR6-spinner magnetometer (AGICO, Brno, Czech Republic).

Analyses with X-ray diffraction (XRD) were performed using bulk and clay samples:

- (1) For X-ray analyses of bulk material, aliquots of 5 g were taken from samples collected in an equidistance of 10 cm and ground in an agate mortar. In order to improve the peak intensity of investigated minerals, carbonate was dissolved at room temperature using acetic acid (10%). The air dried material was then ground again. In order to get semi quantitative mineral contents, 2% Md-IV sulfide was added as a standard (Krischner, 1990). Measurements were performed with a Siemens D 5005 diffractometer at the University of Potsdam with 2 s/point from 4 to 42°2θ, using the Cu-tube FLCu-4KE. Interpretation was executed using MacDiff 4.2.5. software on a Macintosh computer (Petschick, 2000). For analysis, we used the highest peaks of the investigated minerals: For Md-IV-sulfide the molybdenite peak at 14.39°2θ, for quartz the peak at 26.67°2θ, for kaolinite the peak at 12.34°2θ and for illite the peak at 8.84°2θ. The relative amounts of kaolinite and illite were obtained from the ratio mineral/standard of the peak areas. In order to obtain the absolute quartz content, a calibration-curve was constructed using 11 different contents of quartz in an artificial composite of feldspars, muscovite and olivine, spiked with 5% Md-IV-sulfide. The linear regression-curve yields the equation  $y=0.138*x+ 3.07$  ( $R^2=0.99$ ). The intersect  $\neq 0$  reflects that a main-peak of muscovite is close to the investigated quartz-peak. Given that the amount of the various minerals in the standard is constant, this effect was non-significant and the regression quartz/sulphide ( $y=0.138*x$ ) was used for further calculations.
- (2) In order to analyse the clay fraction of selected samples from Femés (50, 170, 205, 485, 525 and 580 cm), aliquots of 7 g were dispersed and the fraction  $b2 \mu\text{m}$  was separated. The suspension was poured on a glass slide allowing the clay minerals to orientate. Measurements were executed at a Seifert XRD C 3000 TT diffractometer (CuK $\alpha$ , 40 kV, 30 mA, 2,5–30,01°2θ; step scan 15,0 s; step size 0,03°) at Dresden University of Technology. Samples were measured three times after each of the following preparation steps: air drying, solvation with ethylene glycol (48 h) and heat

treatment (2 h at 550 °C). Interpretation was completed using the programme Siemens Diffracplus BASIC 4.0#1.

In order to obtain carbonate contents from samples equidistantly sampled every 10 cm, we determined total carbon (TC) and total organic carbon (TOC) contents using an Euro Vector EA3000 Elemental Analyser at GFZ Potsdam/Germany. For TC around 10 mg sample material was wrapped into tin capsules and combusted under oxygen supply at 1000 °C. After combustion, CO<sub>2</sub> was separated in a gas chromatographic column and detected by thermal conductivity. For TOC analysis, around 3 mg of sample material were weighed into Ag-capsules, dropped with 20% HCl, heated for 3 h at 75 °C, finally wrapped in the Ag-capsules and measured with the EA3000. Calibration was performed with the elemental standard “Urea” and verified with a soil reference sample (Boden2). The reproducibility for replicate analyses is 0.2%. Inorganic carbon was calculated by subtraction of organic from total carbon. Finally, carbonate contents were determined by multiplying inorganic carbon contents with a stoichiometric factor of 8.33.

Pedologic analyses at Dresden University of Technology included measurements of pH values, electric conductivity and Na-saturation. We analysed from all three profiles one sample per distinct lithological bed (Fig. 2). In order to determine pH values, 20 g of the samples were mixed with a 0.1 N KCl solution and measured with a pH meter (inoLab, WAW). We determined electric conductivity (EC<sub>5</sub>) by soaking 10 g of sediment in 50 ml of deionized water, filtering the suspension and subsequently determining the conductivity with a conductivity electrode (Tetra Con 325). For measurements of Na-saturation, 10 g of sediment were soaked in a BaCl<sub>2</sub>-triethanolamin solution at pH 8.1 and subsequently filtered. Afterwards, Ca, Na, Mg and K of this filtrate were measured using an Atomic Adsorption Spectrometer (AAS, Analytic Jena vario 6).

Three representative samples (65, 205 and 525 cm) from Femés were investigated for amorphous clay minerals (allophane) following the method of Schlichting et al. (1995): In order to identify the amount of oxalate soluble Al and Si, 1 g air dried material and 50 ml oxalate solution were shaken in darkness for 1 h, and subsequently filtrated. The extraction of dithionite soluble Al and Si was performed using 2 g air dried sample material and 50 ml of a dithionite-citrate solution. Measurements were carried out after treatment with HClO<sub>4</sub> using a flame atomic adsorption spectrometer (Perkin-Elmer) at the University of Gießen/Germany. For micromorphological investigations, undisturbed orientated samples were collected at depths shown in Fig. 2. Following air drying, the blocks were impregnated with Oldopal P80-21. Once hardened, the blocks were cut and polished to 4.8 cm×2.8 cm slices following the

procedure outlined by Beckmann (1997). During preparation, samples were not heated >40 °C. Micromorphological description at the University of Tübingen/Germany follows the terminology of Stoops (2003).

The chronostratigraphy was established using luminescence datings (see Fig. 2), supported by both a correlation between kaolinite contents measured in the valley sediments and nearby marine proxies (kaolinite and iron contents), and by an interprofile stratigraphic correlation between the vegas. Since reliable luminescence datings only cover the period from the Holocene to about 130 ka, the stratigraphy of the lower parts of Femés and Teguisé is based solely on the correlation with marine proxies and the interprofile stratigraphic correlation and thus implies some uncertainty. The chronology is discussed in von Suchodoletz et al. (2008).

## 5. Results

**Grain size:** Although the depth dependent distribution of the ratio clay/<42 µm indicates that ultrasonic treatment prior to laser analysis caused widespread scattering of individual datapoints, a clear temporal signal is recognizable in the underlying trend of the graphs (Figs. 4 and 5 column e). Due to enormous problems in determining the absolute clay content by laser analysis (cf. McCave and Syvitsky, 1991; Konert and Vandenberghe, 1997), only relative estimates are possible. The depth dependent distribution of absolute clay contents from Femés as determined by pipette analyses parallels that of relative clay values obtained using the laser method (Fig. 4), yielding values between 23 and 80%. This demonstrates that despite the lack of absolute clay values the relative results of laser analysis are reliable. This is not disproved by the low correlation coefficient between both curves of only 0.32, since this value is somewhat biased by the large scattering of individual laser data points.

XRD-analyses of bulk samples yield mostly parallel depth dependent distributions of kaolinite and quartz, except for the upper part of Teguisé (Fig. 5 columns g, h). Both show strong variations within one profile, where higher values are generally found in yellowish/silty layers. Absolute quartz contents fluctuate between 6 and 39% in Femés, 4 and 31% in Guatiza III and 7 and 65% in Teguisé (Fig. 5 column h). Due to the lack of a calibration curve, relative instead of absolute kaolinite values must be given. The location of the illite-peaks in the XRD-diffractograms is very close to those of mica which has a similar structure. Thus, illite is not distinguishable from mica. Since mica is exclusively derived from Saharan dust (Coudé-Gaussen et al. 1987; Mizota and Matsuhisa 1995), the proportion of mica/illite is influenced by both pedogenetically formed illite and a change in the composition of the aeolian material.

The latter influence is seen in the partial similarity of the depth dependent distributions of illite/mica, quartz and kaolinite in Guatiza III and in the central part of the Femés profile (Fig. 5 column f).

XRD-analyses of clay samples from Femés (Fig. 6) show a clear peak at 10.0 Å (8.85°2θ), indicating the presence of illite/mica. As mentioned above, a further distinction of illite and mica is not possible. A second prominent peak occurs around 7.16 Å (12.35°2θ), recording the presence of kaolinite. Further secondary peaks of the mentioned clay minerals can be seen. Quartz (3.34 Å) also appears to be ubiquitous. Only some samples (170, 485 and 525 cm) show a faint signal around 15 Å (5.9°2θ) in the air dried record moving towards 16.5 Å (5.4°2θ) after ethylene glycol treatment. This may indicate swellable phyllosilicates, presumably mixed layer minerals.

Environmental magnetic analyses provide both concentration dependent parameters such as initial magnetic susceptibility ( $\kappa$ ) and isothermal remanent magnetisation (IRM), and grain size and mineral specific parameters such as frequency dependent susceptibility ( $\kappa_{fd}$ ) and interparametric ratios, e.g. IRM/ $\kappa$ .  $\kappa$  roughly reflects the bulk amount of magnetic minerals (remanence and non-remanence carrying minerals) in the sediment, whereas IRM reflects only the amount of remanence carriers.  $\kappa_{fd}$  and IRM/ $\kappa$  do not depend on concentration changes at all but provide important information on the composition and grain size distribution of magnetic mineral assemblages.

The measurements yielded high  $\kappa$ - and IRM-values in loess-like yellowish/silty layers, whereas lower values are found in reddish/clayey strata. Absolute values of  $\kappa$  (IRM) vary between 1000 and 5900\*10<sup>-6</sup>SI-units (4–49 A/m) in Teguié, between 2300 and 7400\*10<sup>-6</sup>SI-units (12–97 A/m) in Femés and between 1900 and 8900\*10<sup>-6</sup>SI-units (19–97 A/m) in Guatiza III, respectively (Fig. 5, columns a, b). These extreme values of  $\kappa$  and IRM – at least one order of magnitude higher than those typical for loess or loessic soils in mid latitude settings – indicate that the signal is strongly dominated by ferrimagnetic minerals of detrital origin (e.g. Maher, 1998; Spassov et al., 2003).

Frequency dependent susceptibility ( $\kappa_{fd}$ ), indicating so called superparamagnetic particles, shows a generally anticorrelated pattern to initial magnetic susceptibility and IRM, with highest values in reddish/clayey layers and lowest in yellowish/silty beds. Absolute values vary between 3.7 and 9.4% in Teguié, between 3 and 8% in Femés and between 3.3 and 6% in Guatiza III (Fig. 5, column c). Although the courses of IRM and  $\kappa$  look almost identical, their ratio (IRM/ $\kappa$ ) reveals clear differences. This is expressed by variations on the same wave length as  $\kappa_{fd}$ , but showing an opposite trend. Values range from 5–15 kA/m<sup>-1</sup> in Teguié, from

7–18 kA/m<sup>-1</sup> in Femés and from 10–16 kA/m<sup>-1</sup> in Guatiza III (Fig. 5, column d). Low IRM/ $\kappa$  values in the reddish/clayey layers point to the dominance of non remanence carrying minerals in the magnetic assemblage.

In Fig. 7a, the correlation between  $\kappa$  and IRM is shown. Both parameters are strongly concentration dependent and show a strong linear correlation with distinct grouping of the individual sites. The linear fit shows an intersection  $\neq 0$  with the susceptibility axis. The cross-plot of the frequency dependent susceptibility ( $\kappa_{fd}$ ) to the IRM/ $\kappa$  ratio is displayed in Fig. 7b. These parameters are generally mineral and/or grain size dependent and anticorrelated, with distinct grouping of individual sites.

Overall, the depth-dependent variability of initial magnetic susceptibility ( $\kappa$ ) and IRM with depth is much greater than that of  $\kappa_{fd}$ .  $\kappa$  and IRM show abrupt changes and a wide range of values which are at least partially independent of lithology and/or pedostratigraphy. IRM/ $\kappa$  and  $\kappa_{fd}$ , however, exhibit a more or less regular relationship to depth.

Detailed results of our environmental magnetic investigations will be discussed in a forthcoming paper (Hambach et al., in prep.).

Carbonate contents of the sediment matrix vary between 0% and 47%, highest values showing the Teguisse section. Generally, loess-like layers contain primary carbonate, whereas the matrix of the majority of reddish-clayey layers is non-calcareous (Fig. 5 column i). In the latter, secondary carbonate is found as infillings of cracks and channels.

pH-values in all profiles vary between 7.6 and 8.2, indicating alkaline conditions. An exception is one horizon in Femés (74–120 cm) showing a pH value of 6.6 (Table 2).

Na-saturation varies between 5.8 and 34.2%. Generally, values in Femés show no correlation with indicators of the alternation of loess-like and reddish/clayey material but exhibit a general increase towards the bottom of the profile. In Teguisse, absolute values are generally higher, showing highest values in reddish/clayey layers (Table 2).

Electric conductivity (EC<sub>5</sub>) values are between 70 and 2400  $\mu$ S/cm with highest values found in the profile of Teguisse. This could be explained by the close proximity of this profile to the sea (Table 2). Exemplary analyses for amorphous clay minerals yield a proportion of oxalate-soluble silicon (SiO) below 0.1–0.2%, indicating that amorphous clay minerals are not significant (Table 3) (Dahlgren, 1994).

Micromorphological analyses show well developed pedality, pyroclasts and vitric shards with a different degree of weathering in all thin sections. Grainy peds have a regular size of 20–50  $\mu$ m, mostly compacted to bigger subangular to angular peds (grainy intrapedal microstructure) comparable to the agglomerates of allophane mentioned by Zarei (1989). The depth function

of main micromorphological features can be taken from Table 4, whereas specific features are described and explained below:

**(1) Vega de Femés**

- (a) 108–113 cm: Few thin (around 10  $\mu\text{m}$ ) limpid yellow brown clay coatings indicate clay illuviation, rather more than expected for semi arid climate conditions (Bronger, 1976). At least two redoximorphic phases occurred: (i) granostriated b-fabric around typical and concentric Fe–Mn nodules (mostly  $>100 \mu\text{m}$ ) indicates physical stress (Fig. 8a), attributed to transport or swelling/shrinking processes. These nodules were formed allochthonously and/or the subject to vertic processes. (ii) Ferruginous hypocoatings and aggregate nodules without granostriated b-fabric (Fig. 8a) are younger, since no signs of physical stress are visible. Therefore, we assume that the vertic process is relic.
- (b) 358–363 cm: Fragments of yellow brown clay coatings occurring within non-calcareous peds (Fig. 8b) suggest a formation of clay coatings followed by their destruction. The thickness of these fragments of up to 50  $\mu\text{m}$  in diameter indicates elevated clay illuviation (see chapter 6.2.). Peds and pyroclasts surrounded by non calcareous fine material are embedded in a calcareous micritic groundmass (crystallitic b-fabric) as remnants of a formerly decalcified horizon.
- (c) 498–503 cm: A stipple speckled b-fabric was found only in this section from Femés, indicating neof ormation of clay minerals (Stephan, 2000). Secondary calcification phenomena such as micritic hypocoatings are weakly developed and can generally not be related to distinct palaeoenvironmental changes within the relevant period of time.
- (d) 535–545 cm: Undisturbed yellow brown clay coatings lie next to pressure aggregate surfaces and predate their formation, indicating swelling and shrinking phenomena (Fig. 8c). Fragments of clay coatings within peds denote clay illuviation followed by formation of peds by vertic processes (Fig. 8d). A subangular blocky to crumb microstructure indicates a distinct overprint by bioturbation.

**(2) Vega de Guatiza**

- (a) 450–485 cm: Numerous pyroclasts and vitric shards with voids occur. Most pyroclasts have a small rim of precipitated iron hydroxide as a sign of in situ weathering. Many pyroclasts have inclusions of olivine with no signs of weathering. Limpid yellow brown clay coatings with a thickness of  $\sim 10 \mu\text{m}$  demonstrate weak clay illuviation. Micritic nodules in channels are a result of secondary calcification.

- (b) 510–580 cm: Limpid yellow brown clay coatings represent a first phase of clay translocation. These were often covered by a subsequent secondary calcification corresponding to micritic coatings. Dusty brown clay coatings covering limpid yellow brown clay coatings in compound coatings characterise the second phase of clay illuviation. Locally, complete dense micritic infillings occur with fragments of limpid yellow brown clay coatings.
- (c) 675–730 cm: Silt coatings partly cover dusty yellow brown clay coatings, indicating rapid transport of suspended material. Strongly altered remnants of vitric shards and/or pumice were also apparent somewhat darker than the groundmass (400–500  $\mu\text{m}$  diameter).

### **(3) *Vega de Teguisse***

- (a) 100–120 cm: The occurrence of glauconite shows an influence of marine sediments. Numerous typical manganese–ferruginous nodules with external ferruginous hypocoatings are a result of an in situ redoximorphic phase. Abundant pyroclasts with included unweathered minerals occur only in this thin section. Secondary calcification processes formed micritic hypocoatings predominantly occurring at the lower sides of channels and micritic nodules (up to 500  $\mu\text{m}$  in diameter).
- (b) 142–180 cm: Few limpid yellow brown clay coatings result from weak clay illuviation processes. Abundant tissue and root residues and carbonate pseudomorphs of root cells in channels reveal a distinct influence of rooting. Micritic nodules occur frequently in areas with coarse monic c/f-related distribution that may also be connected to bioturbation. On the other hand, nodules with a higher content of coarse material than the surrounding groundmass (c/f<sub>5  $\mu\text{m}$</sub>  ratio: 1/9) can be regarded as allochthonous.
- (c) 195–220 cm: Two phases of clay illuviation: (i) fragments of 100  $\mu\text{m}$  thick, limpid yellow brown clay coatings represent the older phase, (ii) reddish brown dusty clay coatings the younger phase. Numerous tissue residues, sometimes reddish under plane polarised light, are remnants of rooting and, therefore, bioturbation. Manganese aggregate nodules and ferruginous hypocoatings on groundmass are a result of in situ redoximorphic processes.
- (d) 240–260 cm: Numerous pyroclasts (200–300  $\mu\text{m}$ ) with external ferruginous hypocoatings as well as manganese–ferruginous aggregate nodules can be explained by redoximorphic influence and in-situ weathering. Most of the occurring ferruginous

typical nodules (up to 1.5 mm in diameter) are altered/weathered pyroclasts, therefore, the non-calcareous groundmass seems not to be a weathering product of pyroclasts. Micritic nodules in channels as well as complete dense infillings and micritic hypocoatings on the channel-surrounding groundmass indicate secondary calcification (Fig. 8e).

- (e) 290–350 cm: Channels with dense rims and perpendicular fissures developed similarly to those in 550–590 cm. Microstructure is similar to that in 420–475 cm and 550–590 cm. Nevertheless, the porosity is much higher within the peds than in other thin sections. Strongly altered vitric shards can be found within the groundmass (Fig. 8f).
- (f) 420–475 cm: Channels with dense rims and perpendicular fissures are more distinctly developed than in 550–590 cm. Limpid yellow brown clay coatings (10–20 µm thick) occur within peds. Disorthic typical manganese ferruginous nodules show allochthonous influence, since the size of the included minerals is bigger compared to the minerals in the groundmass (cf. 142–180 cm).
- (g) 550–590 cm: The influence of marine sediments can be demonstrated by the occurrence of numerous glauconites in the groundmass (Fig. 8g). Fissures perpendicular to the walls of channels occur frequently. Channel walls are more compacted than the surrounding groundmass. Limpid yellow brown clay coatings (10–20 µm in thickness) occur within granules. Those intrapedal granules are packed to subangular peds defining a subangular blocky microstructure. During the development of subangular blocky peds, some of the limpid yellow brown clay coatings were fragmented and incorporated into these subangular peds. Locally occurring pressure faces demonstrate weakly developed vertic properties. Vitric shards and pumice are partly strongly weathered, but their shapes are still visible.

## 6. Discussion

### *6.1. Are reddish/clayey layers linked to pedogenesis?*

We intend to use sediment properties for palaeoenvironmental interpretation. For this it is crucial to know if these properties are neoformed by pedogenesis or inherited from Saharan dust which could have changed provenance and thus properties during the Quaternary. Recently collected Saharan dust close to the Canary Islands shows clay contents <15% (Criado and Dorta, 2003; Holz et al., 2004; Menéndez et al., 2007). A slightly weathered Early/Middle Holocene loess-like layer in the Femés section (55–74 cm) contains 23% clay

(Fig. 2, cf. Table 2). Accordingly, in marine sediments ca. 300 km north of Lanzarote, Moreno et al. (2001) observed maximal clay contents of b25% in sediments derived from Saharan dust during the last 250 ka. This indicates that the geogenic clay content inherited from Saharan dust is between 15 and 25%, so that clay contents up to 80% found in the valley sediments must be neoformed on Lanzarote (Table 2).

The extent of pedogenetic processes can be estimated from environmental magnetic properties. Frequency dependent magnetic susceptibility ( $\kappa_{fd}$ ) as well as IRM/ $\kappa$  ratio reflect the proportion of very small superparamagnetic particles newly formed during pedogenesis or, alternatively, produced by weathering controlled maghemitization of local volcanic or aeolian/detrital magnetite derived from Africa (Maher, 1998; Liu et al., 2008). In Fig. 5 (columns a–e) we observe that frequency dependent magnetic susceptibility ( $\kappa_{fd}$ ) and clay content show similar distribution patterns, while initial magnetic susceptibility ( $\kappa$ ), IRM and IRM/ $\kappa$  are generally anticorrelated. Whereas  $\kappa$ , IRM and IRM/ $\kappa$  are increased in the pedogenetically unaltered intervals of the sections and significantly decreased in the soil sediment layers,  $\kappa_{fd}$  exhibits an opposite trend, showing higher values in the soil sediment layers indicating an increased contribution of SP particles here. Interestingly, the relationship of IRM/ $\kappa$  to depth is almost perfectly anti-correlated to  $\kappa_{fd}$ . This can be explained by the greater decrease in remanence in the soil sediment layers as compared to the weaker decay of  $\kappa$ . This observation also points to the relatively increased contribution of SP particles. Values of  $\kappa$  and IRM, found to be very high in loess-like layers probably indicating local volcanic input or a primary ferromagnetic contribution from Saharan dust, are strongly reduced in reddish/clayey strata, indicating a lower concentration of ferromagnetic material here. Although this general pattern can be somewhat biased by a change of volcanic input, as seen in the lower part of Teguse, the general negative correlation with clay contents and  $\kappa_{fd}$  excludes the change of volcanic input to be a main cause for these fluctuations (Fig. 5 columns a, b, c, e). We propose that reduced values of  $\kappa$  and IRM in reddish/clayey layers reflect the transformation of ferromagnetic magnetite/maghemite to less susceptible para- and/or antiferromagnetic phases during rubefication. These environmental magnetic results show that increasing clay contents are paralleled by rubefication processes that are also indicated by the reddish colour of the pedohorizons (see below). This clearly demonstrates that reddish colours of the soil sediment layers (see below) were neoformed on the island and are not inherited from Saharan dust.

As shown by von Suchodoletz et al. (2009), valley base sediments derive from Saharan dust and volcanic material, either deposited as aeolian fallout or as colluvially reworked material

derived from the slopes. Taking the vega of Femés, we find a catchment area/valley base ratio of 5.4:1 (see Table 1), meaning that only 18% of all sediments deposited in the total catchment area were directly deposited as aeolian fallout in the valley base. However, 57% of the total sediment found in the vega system is now stored in the valley base. Thus, most of these sediments were originally deposited and stored somewhere in the catchment area and subsequently colluvially transported into the valley base, yielding a ratio between material deposited as aeolian fallout in the valley base and that deposited as reworked material from the slopes of 1:2.2 or 30:70% (von Suchodoletz et al., 2009). Consequently, most (70%) of the reddish/clayey material found in the vega base must be regarded as soil sediment whose properties are mainly derived from pedogenetic processes active along the slopes. We have to identify ways to discriminate between these properties and those which subsequently formed in the valley base after deposition.

## **6.2. Soil forming processes**

Decalcification is one of the first processes active during pedogenesis. Today, Saharan dust arriving at the Canary Islands contains a carbonate content of about 18–40% (Criado and Dorta, 2003; Menéndez et al., 2007). All studies on recent dust collected north and south of the Sahara detected a certain carbonate content, although material from southern sources contains less carbonate than northern dust (Herrmann et al., 1996; Goudie and Middleton, 2001; Guieu et al., 2002). These findings show that even in case of a change of provenance during the Quaternary Saharan dust deposited on Lanzarote must always have contained a certain proportion of carbonate. The majority of mainly dust-borne soil sediment layers shows a completely decalcified sediment-matrix (Fig. 5, column i). This demonstrates that those sediments which are now alkaline (caused by the presence of carbonate and high salt-content indicated by high electric conductivities) (Table 2) may have been at least slightly acidic along the slopes and in the valley base during pedogenesis as in one horizon from Femés (74–120 cm) showing a pH value below 7. A loess-like layer deposited between 8.5 and 5–2.5 ka in all valleys shows only negligible amounts of carbonate today (Figs. 2 and 5 column i). Since this layer hardly shows other weathering features such as increased clay content and frequency dependent susceptibility, we suggest that similar loess-like layers of Pleistocene age were also decalcified shortly after their deposition on the island. Increased carbonate content in their matrices must hence be caused by secondary recalcification after burial at a later stage of soil formation, when carbonate-rich groundwater was reaching the topmost

sediments of the valley bases. This secondary recalcification is also supported by micromorphological analyses (Fig. 8e).

So-called superparamagnetic grains are found in the magnetic assemblage of soil sediments as indicated by strongly enhanced frequency dependent susceptibility ( $\kappa_{fd}$ ) values. In the cross-plot of Fig. 7a, the correlation between  $\kappa$  and IRM is shown. Both parameters are strongly concentration dependent. The almost perfect linear correlation proves the dependency of the magnetic susceptibility signal on remanence-carrying – probably ferrimagnetic – minerals. The intersections of the linear fits with the susceptibility axis clearly indicate a para- and superparamagnetic contribution to the magnetic susceptibility. The cross-plot of frequency-dependent susceptibility ( $\kappa_{fd}$ ) to IRM/ $\kappa$  is displayed in Fig. 7b. Both parameters are generally mineral and/or grain size dependent, but absolutely independent from variations in concentration. The obvious negative correlation indicates the overall control of the parameters by a non-remanence carrying but highly susceptible mineral fraction. This fraction is most probably composed of superparamagnetic particles derived from weathering of the primarily detrital ferrimagnetic minerals. The distinct grouping of the individual sites gives evidence for the locally variant intensity of pedogenetic processes, in which the more intensive pedogenesis in the profile of Teguisse is explained by its closer position to the sea and thus the greater influence from sea spray.

The loess-like sediments found in the sediment traps on Lanzarote are mainly composed of Saharan dust with a minor contribution of local volcanic fallout, both either directly deposited as aeolian fallout or as hill-wash material (von Suchodoletz et al., 2009). These sediments underwent intense pedogenesis during humid periods which also affected the magnetic minerals. The unaltered magnetic mineralogy of the loess-like sediments stems from Saharan dust, occasionally from volcanic fallout and regularly from the additive of local volcanic material derived from the erosion of the volcanic rocks of the island. This magnetic mineralogy is probably characterised by magnetite/maghemite in a grain size distribution lying within the superparamagnetic/single domain (SP/SD) range with significant proportions in both parts (Hambach et al., in preparation). During more humid periods, when pedogenesis prevails, low temperature oxidation of primarily detrital magnetite to maghemite and/or the neo-formation of superparamagnetic particles formed by dehydration of pedogenic ferrihydrite shift the grain size distribution slightly to the SP range (Liu et al., 2008). The presence of SD bacterial magnetite, which suffered the same fate, cannot be excluded. The resulting magnetic grain assemblage shows significant lower remanence, slightly lower initial susceptibility, but increased  $\kappa_{fd}$  (compare Fig. 5a, b, c). Thus, we are facing the relative

increase of the SP-grain-size-fraction at the expenses of the SD-fraction. This observation can be solely explained by processes affecting a quite homogenous primary magnetic mineralogy in a setting of varying pedogenetic intensity with time.

As mentioned above, pedogenesis is characterised by a strong neoformation of clay minerals, increasing the content of clay up to 80%. The volcanic environment of Lanzarote facilitates a steady supply of dissolved cations in ground and slope water. Cations are not directly leached due to the semi-arid climate (Zarei, 1989). These are ideal conditions for a formation of smectite, as reported from soils in a similar environment in Central Mexico (Solleiro-Rebolledo et al., 2003) and from soils on Lanzarote (Jahn, 1988; Zarei, 1989). For testing the presence of smectite in the sediments found in the valley floor, we performed XRD analyses of the clay fraction from the Femés section. A colluvium sample (50 cm) was composed of material derived from a loess-like layer originating from the Early/Middle Holocene (cf. Figs. 2 and 5 column e), showing a clay content of 23% (Table 2). This sample is mainly composed of kaolinite and illite and shows no smectite, confirming the minor smectite content of Saharan dust (Criado and Dorta, 2003; Holz et al., 2004; Menéndez et al., 2007). Five samples were collected from layers showing medium to high clay contents between 23 and 77% (170, 205, 485, 525 and 580 cm; cf. Fig. 5 column e). But, unlike the results of Zöller et al. (2004) who found a significant proportion of smectite in the profile of Femés, only small amounts were detected here (Fig. 6). The absence of large quantities of smectite is confirmed by parallel XRD analyses of the clay fraction of four samples (50, 170, 485, 580 cm) performed at the USGS in Boulder/USA. Obviously, the formation of smectite is not the main cause for high clay content in the valley base sediments.

Other clay minerals such as illite, kaolinite and chlorite are abundant, but also frequently found in Saharan dust (Coudé-Gaussen, 1987; Caquineau et al., 1998; Menéndez et al., 2007). Accordingly, they are regularly observed in slightly weathered loess-like layers of the valley base sediments (for kaolinite and illite see Fig. 5 columns f, g). However, Zarei (1989) hypothesizes that all these clay minerals could also have formed during weathering. Nevertheless, strong in situ formation of illite is unlikely because there is no general relationship between illite/mica and the indicators of pedogenesis such as frequency dependent susceptibility or clay content (Fig. 5 columns c, e, f). Only in Teguiwe we can see some similar trends indicating some neoformation during pedogenesis. The occurrence pattern of kaolinite is largely parallel to that of quartz (Fig. 5 columns f, g). Quartz has a completely aeolian origin since it does not form from the weathering of basaltic rock (Jahn, 1995; Mizota

and Matsuhisa, 1995). The close similarity of quartz and kaolinite suggests that it is unlikely that the latter was formed in the soils of Lanzarote. This is supported by Bronger and Sedov (2003) who found no neoformation of kaolinite in terrae rossa (Rhodoxeralfs) developing from the Middle Pleistocene until today at the SW coast of Morocco, in climatic conditions similar to those on Lanzarote. Clay minerals such as chlorite can hardly be distinguished from montmorillonite and vermiculite, because they appear rather diffuse in the diffractograms. Since Zarei (1989) reported only a rare occurrence of chlorite on Lanzarote, it is obviously not largely formed here.

Clay minerals such as allophane and halloysite described in former studies (Zarei, 1989) could not be detected in XRD-diffractograms due to the fact that they are X-ray amorphous. Zarei (1989) describes these minerals from a horizon with an age of around 21 ka (formerly called series IV<sub>A</sub>, Carracedo et al., 2003), and attributed them to weathering of volcanic glass in soils. Direct weathering of pyroclasts to clay could be observed by micromorphology in our profiles (cf. chapter 4, Fig. 8f). Weathering features on the surfaces of volcanic material even in slightly weathered loess-like horizons show that this process starts already very early during pedogenesis. Weathering of volcanic material can also be tracked by a lowering of initial magnetic susceptibility  $\kappa$  in soil sediments as described above and seen in Fig. 5 (column a). Zarei (1989) describes the formation of subangular to round dark-brown microaggregates with an average size of 10–50  $\mu\text{m}$  in soil horizons showing high amounts of allophane, oxides and hydroxides on Lanzarote. We also found large amounts of similar aggregates in clay rich soil sediment layers characterised by shrinking and swelling (Fig. 3). In conclusion, these observations suggest that XRD- amorphous clay should have formed in the valley base soils of Lanzarote. However, analyses of three samples (two showing high clay contents) from Femés did not indicate its presence (Table 3).

Clay Illuviation is traceable by clay coatings found in thin sections and occurred during periods of pedogenesis along the slopes as well as in the valley bases (Tables 2 and 4). However, those coatings formed on the slopes were destroyed during colluvial transport and are only preserved as fragments in the valley base sediments (Fig. 8b). Dispersion and transportation of clay from the palaeosurface downwards were easily facilitated by high sodium saturation caused by sea spray, destabilizing the soil structure (Table 2, Jahn, 1988). Furthermore, soluble salts as found in large quantities (high electric conductivities, cf. Table 2) were probably washed away since they would have inhibited the dispersion of clay. Thus, this process cannot directly be compared to clay illuviation processes found e.g. in Central Europe, where they indicate special environmental conditions (e.g. Kühn et al., 2006).

The majority of soil-sediment layers exhibit a strong vertic texture. Periods of shrinking and swelling are reported by slickensides and vertical cracks at different scales, observed in outcrops and in thin sections (Figs. 8a,c and 9, Table 2). Most commonly, smectite produces vertic features in soils (Duchaufour, 1982; Nordt et al., 2004), but allophane may also cause shrinking and swelling (Wan et al., 2002). Intense vertic properties demonstrate that either smectite or amorphous clay minerals must be present in larger amounts, being responsible for high clay contents in soil-derived horizons. Yet, it is not clear why analyses show converse results (see above). Consequently, the solution to this problem requires further investigation. The smooth courses of frequency dependent susceptibility ( $\kappa_{fd}$ ) and IRM/ $\kappa$  reflect in situ pedogenetic processes. They clearly demonstrate that they were not affected by the vertic processes reaching depths as large as 100 cm described in other studies (e.g. Kovda et al., 2001). The smooth pattern, however, is in contrast to the pattern of initial magnetic susceptibility ( $\kappa$ ) controlled by the primary mixture of Saharan dust and local volcanic material, characterised by abrupt changes in its depth dependent function.

Strong rubefication as indicated by Munsell-colors in the range of 2.5 YR and 5 YR in the soil sediments (cf. Schwertmann et al., 1982; Michalet et al., 1993) is contemporaneous to the formation of superparamagnetic particles and clay minerals (see above). Michalet et al. (1993) demonstrate that in Moroccan soils the formation of clay microaggregates such as those found in the soil sediments of the vegas (see above) generally favours the rubefication process. Rubefication causes the dark-red colour of the soil sediments, in contrast to the yellowish colour of slightly weathered loess-like layers. This process is typical for seasonally humid tropic and subtropic soils and occurs in a slightly acidic/neutral milieu, thus confirming an early decalcification of the sediments shortly after their deposition (Zech and Hintermaier-Erhard, 2002).

Iron–manganese nodules of different size and hypocoatings on ped surfaces (Fig. 8a) indicate strong redoximorphic dynamics in the valley base sediments. Polygenetic neof ormation of ferromanganese features (Fig. 8a) within one layer and their disappearing upslope suggest that these dynamics take mainly place in valley base environments, probably beginning during sedimentation and lasting until today.

### **6.3. Palaeoenvironmental conditions as inferred from pedogenetic proxies**

Luminescence datings show that soil sediment layers generally have similar sedimentation rates as slightly weathered loess-like horizons (von Suchodoletz et al., 2008). Therefore, differences in the intensity of pedogenetic properties are mainly caused by a change of

climate conditions rather than by variation in the time span available for pedogenesis (Busacca and Cremaschi, 1998; Sedov et al., 2003; Faust and Haubold, 2007). Since the climate of Lanzarote is semiarid, the main factor limiting pedogenesis is humidity. Hence, soil properties can yield information about palaeoedaphic moisture conditions.

We have demonstrated that pedogenetic processes may take place along slopes and to some degree in the valley bases. Consequently, only some of the pedogenetic features observed in the valley base sediments can be used as indicators for primary pedogenesis and may therefore be useful palaeoenvironmental proxies. From genetic relationships and analysis we would classify some characteristics as primary pedogenetic features, more or less contemporaneous to the first material deposition in the vega catchments. Some of these can be traced by proxies: (i) vertic processes (as evidenced by outcrop and micromorphological investigations; Table 2, Fig. 10 column a) (ii) clay mineral formation (clay contents; Fig. 10, column b) (iii) formation of superparamagnetic minerals linked with rubefication (traceable with frequency dependent susceptibility; Fig. 10 column c), and (v) clay illuviation. The vertic processes information was combined with the rate of occurrence of calcified anthophora-bee nests as direct indicators of soil moisture, leading to a combined soil moisture proxy (Fig. 10 column a). Due to the lack of continuous micromorphological samples, clay illuviation cannot be traced. Furthermore, due to its fostering by high Na-saturation it is not useful as a palaeoenvironmental proxy here. As shown above (Section 6.2), vertic processes occurred a very short time after deposition into the vega base, and the other processes predominantly took place on the slopes prior to erosion. These processes have to be separated from processes restricted to later stages of pedogenesis of uncertain duration, overprinting primary pedogenetic features of soils and soil sediments in the valley bases. Such subsequent processes are the mobilisation of Fe and Mn and carbonate dissolution or precipitation. With a few singular exceptions (e.g. in Teguisse 388–408 cm), soil moisture (derived from vertic properties and the occurrence of anthophora bee nests), clay contents and frequency dependent susceptibility show parallel depth dependent functions, increasing in soil-sediment layers and decreasing in less weathered loess-like material. Altogether, these proxies display a coherent isochronous pattern of pedogenetic intensity exclusively controlled by climate (enhanced soil moisture). The chronological evidence, when considered alongside the correlating patterns across vegas, indicate general robust support of a soil moisture pattern based on pedogenesis. These results show that parts of MIS 2, 3, 4 and 6 exhibited higher soil moisture levels than today, whereas most parts of MIS 1 and 5 were obviously as dry or even

drier when compared to recent conditions. In general, cold periods were obviously characterised by moisture, and warm periods by drier conditions (Fig. 10). Furthermore, the occurrence of fossilised nests of anthophora-bees can provide some hints about precipitation intensity (Table 3). The nests occur almost exclusively in weakly developed soil sediments showing clay contents between 26 and 63% in Femés (Table 2), and were formed during slightly moister periods compared to today (Figs. 2 and 10). According to Edwards and Meco (2000) and Genise and Edwards (2003) these bees thrive during periods of increased precipitation in semiarid areas with 200 to 500 mm annual precipitation, slightly above the actual rainfall rates of 100 to 200 mm a<sup>-1</sup> (Jahn, 1988). The bees probably inhabited these environments when precipitation reached 200 to 300 mm a<sup>-1</sup>. It is likely that they had left the nests already before reaching their upper ecological humidity limit of 500 mm a<sup>-1</sup>, presumably caused by something similar to the seasonal lagoons reported prior to the 15<sup>th</sup> century here (Santana-Santana, 2003), with stagnant water collecting in the valleys and covering the valley centres. Since anthophora bee nests are not found in strongly developed soil-sediments, it is evident that strong soil formation with rubefication and clay formation must have happened under climatic conditions of more than 300 mm annual precipitation. While ground-nesting bees indicate that the moisture regime during periods of slight pedogenesis on Lanzarote were a little more intensive than today, we can estimate the humidity range during periods of strong pedogenesis through recent soil forming processes described in a catena in Tenerife covering the last 10 ka (Fernandez-Caldas et al., 1981): Today, brunification, rubefaction and the formation of amorphous allophane and smectite occur in a comparable geological situation attributed to climatic conditions with precipitation up to 560 mm (Kämmer, 1974). However, soil moisture is influenced by various factors such as cloudiness, air temperature and precipitation, and these soils from Tenerife are found in a region that has on the one hand strong cloud cover and on the other hand a mean annual temperature below that of Lanzarote. Thus, this value is not directly comparable to past conditions on Lanzarote. Nevertheless, it can give about a reasonable estimate of the water budget on Lanzarote during more humid periods of the Quaternary. Altogether, the water budget was obviously more positive during most parts of the investigated time period, namely during glacial stages.

## **7. Conclusions**

Using grain size analyses, environmental magnetic investigations, micromorphology and pedological analyses, we could support the hypothesis that reddish/clayey layers in valley

base sediments on Lanzarote are derived from local palaeosols. These palaeosols were formed by various pedogenetic processes such as clay formation and rubefication during periods of enhanced soil moisture in the valley bases and especially along the slopes. Subsequently, the material derived from the slopes was transported to the valley bases by colluvial processes during low amplitude and high frequency sedimentation events, so that the layers consist of soil sediments rather than in situ soils. Using clay contents, environmental magnetic parameters, palaeontological remains and the occurrence of vertic properties, a chronology of periods with enhanced soil moisture could be established for the Late Quaternary. This chronology demonstrates that cold periods like parts of MIS 2, 3 and 4 and 6 were characterised by a higher soil moisture than currently, whereas most parts of warm MIS 1 and 5 were obviously as dry or even drier than today. Since various factors influence soil moisture, it is not possible to derive palaeoprecipitation values from these valley base sediment samples directly. However, using palaeontological findings and a comparison with recent soils on Tenerife, rough estimations are possible. These show that maximal soil moisture corresponds to that found in regions of Tenerife with a recent precipitation of up to  $560 \text{ mm a}^{-1}$ ; however, a direct comparison with this value is not possible due to the variance in climatic conditions between both islands as well as between glacials and the recent period. Since most parts of the profiles consist of soil sediments rather than loess-like material, the water budget of Lanzarote was obviously more positive during most parts of the investigated time period. Hence, the recent dry climate of Lanzarote is rather an exception than the rule.

### **Acknowledgements**

The work of the first author was funded for two years by a postgraduate grant of the Free State of Bavaria, Germany, supplied by the University of Bayreuth. Further financial support was given by Deutsche Forschungsgemeinschaft (project Zo 51/29-1).

We are indebted to Dan Muhs (USGS Boulder, CO/USA) for comparative XRD analyses of clay minerals. Furthermore, we thank Beate Mocek and Max Wilke (University of Potsdam/Germany) for help during XRD analyses of bulk samples, Birgit Plessen (GFZ Potsdam/Germany) for her support during carbonate analyses and Georg Schettler (GFZ Potsdam/Germany) for facilitating grain size analyses. We thank Peter Felix-Henningsen (University of Gießen/Germany) for allophane analyses. For help during grain size analyses we are grateful to Gert Herold, David Sonnabend and Sebastian Breitenbach (all GFZ Potsdam/Germany). We thank Hedi Oberhänsli (GFZ Potsdam/Germany) for a critical revision of structure and language of the manuscript. The Student's Parish of the Catholic

University Eichstätt/Germany is thanked for offering conference facilities. We thank John Dearing (University of Liverpool) and an anonymous reviewer for their helpful critiques, and Fiona Mulvey (Technical University of Dresden/Germany) for a strong improvement of the English manuscript.

## References

- Aléon, J., Chaussidon, M., Marty, B., Schütz, L., Jaenicke, R. (2002): Oxygen isotopes in single micrometer-sized quartz grains: tracing the source of Saharan dust over long-distance atmospheric transport. *Geochimica et Cosmochimica Acta* 66/19, 3351–3365.
- Antoine, P., Rousseau, D.-D., Zöller, L., Lang, A., Munaut, A.-V., Hatté, C., Fontugne, M. (2001): High-resolution record of the last interglacial–glacial cycle in the Nussloch loess–palaeosol sequences, Upper Rhine Area, Germany. *Quaternary International* 76–77, 211–229.
- Beckmann, T. (1997): Präparation bodenkundlicher Dünnschliffe für mikromorphologische Untersuchungen. *Hohenheimer Bodenkundliche Hefte* 40, 89–103.
- Bozzano, G., Kuhlmann, H., Alonso, B. (2002): Storminess control over African dust input to the Moroccan Atlantic margin (NWAfrica) at the time of maxima boreal summer insolation: a record of the last 220 kyr. *Palaeogeography, Palaeoclimatology, Palaeoecology* 183, 155–168.
- Bronger, A. (1976): Zur quartären Klima- und Landschaftsentwicklung des Karpatenbeckens auf (paläo-) pedologischer und bodengeographischer Grundlage. *Kieler Geographische Schriften* 45. 268 pp.
- Bronger, A., Heinkele, T. (1989): Micromorphology and genesis of paleosols in the Luochuan loess section, China: podostratigraphic and environmental implications. *Geoderma* 45/2, 123–143.
- Bronger, A., Sedov, S.N. (2003): Vetusols and paleosols: natural versus man-induced environmental change in the Atlantic coastal region of Morocco. *Quaternary International* 106/107, 33–60.
- Busacca, A., Cremaschi, M. (1998): The role of time versus climate in the formation of deep soils of the Apennine Fringe of the Po valley, Italy. *Quaternary International* 51/52, 95–107.

- Bush, A.B.G., Little, E.C., Rokosh, D., White, D., Rutter, N.W. (2004): Investigation of the spatio-temporal variability in Eurasian Late Quaternary loess–paleosol sequences using a coupled atmosphere–ocean general circulation model. *Quaternary Science Reviews* 23, 481–498.
- Caquineau, S., Gaudichet, A., Gomes, L., Magonthier, M.-C., Chatenet, B. (1998): Saharan dust: Clay ratio as a relevant tracer to assess the origin of soil-derived aerosols. *Geophysical Research Letters* 25/7, 983–986.
- Carracedo, J.C., Day, S., Guillou, H., Rodríguez-Badiola, E., Canas, J.A., Pérez-Torrado, F.J. (1998): Hotspot volcanism close to a passive continental margin: the Canary Islands. *Geological Magazine* 135/5, 591–604.
- Carracedo, J.C., Singer, B., Jicha, B., Guillou, H., Rodríguez-Badiola, E., Meco, J., Pérez-Torrado, J., Gimeno, D., Socorro, S., Láinez, A. (2003): La erupción y el tubo volcánico del volcán Corona (Lanzarote, Islas Canarias). *Estudios Geológicos* 59, 277–302.
- Carter-Stiglitz, B., Banerjee, S.K., Gurlan, A., Oches, E. (2006): A multi-proxy study of Argentina loess: marine oxygen isotope stage 4 and 5 environmental record from pedogenic hematite. *Palaeogeography, Palaeoclimatology, Palaeoecology* 239, 45–62.
- Coello, J., Cantagrel, J.-M., Hernán, F., Fúster, J.-M., Ibarrola, E., Ancochea, E., Casquet, C., Jamond, C., de Téran, J.-R.D., Cendrero, A. (1992): Evolution of the eastern volcanic ridge of the Canary Islands based on new K–Ar data. *Journal of Volcanology and Geothermal Research* 53, 251–274.
- Coudé-Gaussen, G. (1991): *Les poussières sahariennes*. Edition John Libbey Eurotext, Paris. 485 pp.
- Coudé-Gaussen, G., Rognon, P., Bergametti, G., Gomes, L., Strauss, B., Gros, J.M., le Coustumer, M.N. (1987): Saharan dust of Fuerteventura island (Canaries): chemical and mineralogical characteristics, air mass trajectories, and probable sources. *Journal of Geophysical Research* 92/D8, 9753–9771.
- Criado, C., Dorta, P. (2003): An unusual ‘blood rain’ over the Canary Islands (Spain). The storm of January 1999. *Journal of Arid Environments* 55, 765–783.
- Dahlgren, R.A. (1994): Quantification of allophane and imogolite. *Quantitative Methods in Soil Mineralogy*. SSSA Miscellaneous Publications, Madison, WI, pp. 430–450.
- Dearing, J.A., Livingstone, I.P., Bateman, M.D., White, K. (2001): Palaeoclimate records from OIS 8.0–5.4 recorded in loess–paleosol sequences on the Matmata Plateau,

- southern Tunisia, based on mineral magnetism and new luminescence dating. *Quaternary International* 76/77, 43–56.
- Dodonov, A.E., Baiguzina, L.L. (1995): Loess stratigraphy of Central Asia: Palaeoclimatic and palaeoenvironmental aspects. *Quaternary Science Reviews* 14 (7–8), 707–720.
  - Duchaufour, P. (1982): *Pedology. Pedogenesis and Classification*. George Allen & Unwin, London.
  - Edwards, N., Meco, J. (2000) Morphology and palaeoenvironment of brood cells of Quaternary ground-nesting solitary bees (Hymenoptera, Apidae) from Fuerteventura, Canary Islands, Spain. *Proceedings of the Geologist's Association* 111, 173–183.
  - Evans, M.E., Heller, F. (2003): *Environmental Magnetism — Principles and Applications of Enviromagnetics*. Academic Press. 299 pp.
  - Fassbinder, J.W.E., Stanjek, H., Vali, H. (1990): Occurrence of magnetic bacteria in soil. *Nature* 343, 161–163.
  - Faust, D., Haubold, F. (2007): Was können Böden uns verraten? *Local Land and Soil News* 20/21, 13–15.
  - Fernandez-Caldas, E., Quantin, P., Tejedor-Salguero, M.L. (1981): Séquences climatiques des sols dérivés des roches volcaniques aux Iles Canaries. *Geoderma* 26, 47–62.
  - Genise, J.F., Edwards, N. (2003): Ichnotaxonomy, origin, and paleoenvironment of Quaternary insect cells from Fuerteventura, Canary Islands, Spain. *Journal of the Kansas Entomological Society* 76/2, 320–327.
  - Goudie, A.S., Middleton, N.J. (2001): Saharan dust storms: nature and consequences. *Earth-Science Reviews* 56, 179–204.
  - Guieu, C., Loyer-Pilot, M.-D., Ridame, C., Thomas, C. (2002): Chemical characterization of the Saharan dust end-member: some biogeochemical implications for the western Mediterranean Sea. *Journal of Geophysical Research* 107, 2002, d15, ACH5.1–ACH5.11.
  - Hambach, U., Rolf, C., Schnepf, E. (2008): Magnetic dating of Quaternary sediments, volcanites and archaeological materials: an overview. *Eiszeitalter und Gegenwart. Quaternary Science Journal* 57, 25–51.
  - Hatté, C., Antoine, P., Fontugne, M., Lang, A., Rousseau, D.-D., Zöller, L. (2001):  $\delta^{13}\text{C}$  of loess organic matter as a potential proxy for paleoprecipitation. *Quaternary Research* 55, 33–38.

- Heinkele, T. (1990): Bodengeographische und paläopedologische Untersuchungen im zentralen Lössplateau von China — ein Beitrag zur quartären Klima- und Landschaftsgeschichte. Schriftenreihe des Instituts für Pflanzenernährung und Bodenkunde der Universität Kiel 9, 120 pp.
- Helgeson, H.C., Murphy, W.M., Aargaard, P. (1984): Thermodynamic and kinetic constraints on reaction rates among minerals and aqueous solutions. II. Rate constants, effective surface area, and the hydrolysis of feldspar. *Geochimica et Cosmochimica Acta* 48, 2405–2432.
- Herrmann, R., Jahn, R., Stahr, K. (1996): Identification and quantification of dust additions in perisaharan soils. In: Guerzoni, R., Chester, R. (Eds.), *The Impact of Desert Dust Across the Mediterranean*. Kluwer Academic Press, pp. 173–182.
- Holz, C., Stuut, J.B., Henrich, R. (2004): Variability in terrigenous sedimentation processes off NW Africa and its relation to climate changes: inferences from grain-size distributions of a Holocene marine sediment record. *Sedimentology* 51/5, 1145–1154.
- Jahn, R. (1988): Böden Lanzarotes. PhD-thesis, Stuttgart-Hohenheim, 175 pp.
- Jahn, R. (1995): Ausmaß äolischer Einträge in circumsaharischen Böden und ihre Auswirkungen auf Bodenentwicklung und Standortseigenschaften. Habilitation, Stuttgart-Hohenheim. 175 pp.
- Instituto Tecnológico y Geominero de España (2005): Mapa geológico de España, Escala 1: 100.000, Memoria de la hoja geológica de la Isla de Lanzarote. Madrid. ISBN: 84-7840-606-
- Junfeng, J., Jun, C., Huayu, L. (1999): Origin of illite in the loess from the Luochuan area, Loess Plateau, central China. *Clay Minerals* 34/4, 525–532.
- Kämmer, F. (1974): Klima und Vegetation auf Tenerife, besonders im Hinblick auf den Nebelniederschlag. *Scripta Geobotanica*, vol. 7. Göttingen. 78 pp.
- Konert, M., Vandenberghe, J. (1997): Comparison of laser grain size analysis with pipette and sieve analysis: a solution for the underestimation of the clay fraction. *Sedimentology* 44, 523–535.
- Koopmann, B. (1981): Sedimentation von Saharastaub im subtropischen Nordatlantik während der letzten 25 000 Jahre. *Meteor Forschungsergebnisse C/35*, 23–59.
- Kovda, I., Lynn, W., Williams, D., Chichagova, O. (2001): Radiocarbon age of vertisols and its interpretation using data on gilgai complex in the North Caucasus. *Radiocarbon* 43, 603–609.

- Krischner, H. (1990): Einführung in die Röntgenfeinstrukturanalyse. Edition Vieweg, Braunschweig. 193 pp.
- Kühn, P., Billwitz, K., Bauriegel, A., Kühn, D., Eckelmann, W. (2006): Distribution and genesis of Fahlerden (Albeluvisols) in Germany. *Journal of Plant Nutrition and Soil Science* 169, 420–433.
- Kunkel, G. (1993): Die Kanarischen Inseln und ihre Pflanzenwelt. Edition Fischer, Stuttgart, Jena, 230 pp.
- Langbein, W.B., Schumm, S.A. (1958): Yield of sediment in relation to mean annual precipitation. *Transactions of the American Geophysical Union* 39/6, 1076–1084.
- Liu, Q., Barrón, V., Torrent, J., Eeckhout, S.G., Deng, C. (2008): Magnetism of intermediate hydromaghemite in the transformation of 2-line ferrihydrite into hematite and its palaeoenvironmental implications. *Journal of Geophysical Research* 113, B01103. doi:10.1029/2007JB005207.
- Maher, B.A. (1998): Magnetic properties of modern soils and Quaternary loessic paleosols: paleoclimatic implications. *Palaeogeography, Palaeoclimatology, Palaeoecology* 137, 25–54.
- Maher, B.A., Thompson, R. (1992): Paleoclimatic significance of the mineral magnetic record of the Chinese loess and paleosols. *Quaternary Research* 37, 155–170.
- Maher, B.A., Alekseev, A., Alekseeva, T. (2002): Variation of soil magnetism across the Russian steppe: its significance for use of soil magnetism as a palaeorainfall proxy. *Quaternary Science Reviews* 21, 1571–1576.
- Markovic, S.B., Hambach, U., Catto, N., Jovanovic, M., Buggle, B., Machalett, B., Zöller, L., Glaser, B., Frechen, M. (2008): Middle and Late Pleistocene loess sequences at Batajnica, Vojvodina, Serbia. *Quaternary International* 198, 255–266.
- McCave, I.N., Syvitsky, J.P.M. (1991): Principles and methods of geological particle size analysis. In: Syvitsky, J.P.M. (Ed.), *Principles, Methods, and Application of Particle Size Analysis*. Cambridge University Press, pp. 3–21.
- Menéndez, I., Diaz-Hernandez, J.L., Mangas, J., Alonso, I., Sanchez-Soto, P.-J. (2007): Airborne dust accumulation and soil development in the North-East sector of Gran Canaria (Canary Islands, Spain). *Journal of Arid Environments* 71, 57–81.
- Michalet, R., Guillet, B., Souchier, B. (1993): Hematite identification in pseudoparticles of Moroccan rubified soils. *Clay Minerals* 28, 233–242.

- Mizota, C., Matsuhisa, Y. (1995): Isotopic evidence for the eolian origin of quartz and mica in soils developed on volcanic materials in the Canary Archipelago. *Geoderma* 66, 313–320.
- Moreno, A., Taragona, J., Henderiks, J., Canals, M., Freudenthal, T., Meggers, H., (2001): Orbital forcing of dust supply to the North Canary Basin over the last 250 kyr. *Quaternary Science Reviews* 20, 1327–1339.
- Nordt, L.C., Wilding, L.P., Lynn, W.C., Crawford, C.C. (2004): Vertisol genesis in a humid climate of the coastal plain of Texas, U.S.A. *Geoderma* 122, 83–102.
- Petschick, R. (2000): MacDiff 4.2.5. Manual. [http://www.geologie.uni-frankfurt.de/Staff/Homepages/Petschick/PDFs/MacDiff\\_Manual\\_D.pdf](http://www.geologie.uni-frankfurt.de/Staff/Homepages/Petschick/PDFs/MacDiff_Manual_D.pdf).
- Prospero, J.M., Lamb, P.J. (2003): African droughts and dust transport to the Caribbean: climate change implications. *Science* 302, 1024–1027
- Rothe, P. (1996): Kanarische Inseln. Edition Gebrüder Bornträger Berlin, Stuttgart, 307 pp.
- Santana-Santana, A. (2003): Consideraciones en torno al medio natural canario anterior a la conquista. *Eres (Arqueología/Antropología)* 11, 61–75.
- Schellenberger, A., Veit, H. (2006): Pedostratigraphy and pedological and geochemical characterization of Las Carreras loess–paleosol sequence, Valle de Tafi, NW Argentina. *Quaternary Science Reviews* 25, 811–831.
- Schlichting, E., Blume, H.-P., Stahr, K. (1995): *Bodenkundliches Praktikum*, Pareys Studentexte 81, Edition Blackwell Wissenschaft, Berlin, 295 pp.
- Schüle, J., Stahr, K., Zarei, M., Jahn, R. (1989): Basaltverwitterung und Bodenentwicklung seit dem mittleren Tertiär auf Lanzarote, Kanarische Inseln (Profil Malaya Chica). *Zeitschrift für Pflanzenernährung und Bodenkunde* 152, 105–113.
- Schwertmann, U., Murad, E., Schulze, D.G. (1982): Is there Holocene reddening (hematite formation) in soils of axeric temperate areas? *Geoderma* 27, 209–223.
- Sedov, S., Solleiro-Rebolledo, E., Morales-Puente, P., Arias-Herreia, A., Vallejo-Gómez, E., Jasso-Castaneda, C. (2003): Mineral and organic components of the buried paleosols of the Nevado de Toluca, Central Mexico as indicators of paleoenvironments and soil evolution. *Quaternary International* 106/107, 169–184.
- Solleiro-Rebolledo, E., Sedov, S., Gama-Castro, J., Flores-Román, D., Escamilla-Sarabia, G. (2003): Paleosol-sedimentary sequences of the Glacis de Buenavista, Central Mexico: interaction of Late Quaternary pedogenesis and volcanic sedimentation. *Quaternary International* 106/107, 185–201.

- Spassov, S., Heller, F., Kretzschmar, R., Evans, M.E., Yue, L.P., Nourgaliev, D.K., (2003): Detrital and pedogenic magnetic mineral phases in the loess/palaeosol sequence at Lingtai (Central Chinese Loess Plateau). *Physics of the Earth and Planetary Interiors* 140, 255–275.
- Stephan, S. (2000.): Bt-Horizonte als Interglazial-Zeiger in den humiden Mittelbreiten: Bildung, Mikromorphologie, Kriterien. *Eiszeitalter und Gegenwart* 50, 95–106.
- Stoops, G. (2003): Guidelines for Analysis and Description of Soil and Regolith Thin Sections. Soil Science Society of America, Madison, WI. 184 pp.
- Torrent, J., Barrón, V., Liu, Q. (2006): Magnetic enhancement is linked to and precedes hematite formation in aerobic soils. *Geophysical Research Letters* 33, L02401. doi:10.1029/2005GL024818.
- van Velzen, A.J., Dekkers, M.J. (1999): Low-temperature oxidation of magnetite in loess paleosol sequences: a correction of rock magnetic parameters. *Studia Geophysica et Geodaetica* 43/4, 357–375.
- von Suchodoletz, H., Fuchs, M., Zöller, L. (2008): Dating Saharan dust deposits at Lanzarote (Canary Islands) by luminescence dating techniques and their implication for paleoclimate reconstruction of NW Africa. *Geochemistry, Geophysics, and Geosystems* 9. doi:10.1029/2007GC001658.
- von Suchodoletz, H., Faust, D., Zöller, L. (2009): Geomorphological investigations of sediment traps on Lanzarote (Canary Islands) as a key for the interpretation of a palaeoclimate archive off NW Africa. *Quaternary International* 196, 44–56.
- Walden, J., Oldfield, F. & Smith, J.P. (1999): Environmental magnetism: a practical guide. Technical Guide Series 6, Quaternary Research Association, 250 pp.
- Wan, Y., Kwong, J., Brandes, H.G., Jones, R.C. (2002): Influence of amorphous clay-size materials on soil plasticity and shrink–swell behaviour. *Journal of Geotechnical and Geoenvironmental Engineering* 128/12, 1026–1031.
- Wright, J.S. (2001): “Desert” loess versus “glacial” loess: quartz silt formation, source areas and sediment pathways in the formation of loess deposits. *Geomorphology* 36, 231–256.
- Yaalon, D., Bruins, H.J. (1977): Sediments and paleosols as indicators of climatic fluctuations in the loessial desert fringe of the Negev, Israel, Proc. X. INQUA Cong., Birmingham, 507.
- Zarei, M. (1989): Verwitterung und Mineralneubildung in Böden aus Vulkaniten auf Lanzarote (Kanarische Inseln). Edition B. Schulz Berlin, 255 pp.

- Zech, W., Hintermaier-Erhard, G. (2002): Böden der Welt. Edition Spektrum Akademischer Verlag Heidelberg, Berlin, 113 pp.
- Zöller, L., von Suchodoletz, H., Küster, N. (2003): Geoarchaeological and chronometrical evidence of early human occupation on Lanzarote (Canary Islands). *Quaternary Science Reviews* 22, 1299–1307.
- Zöller, L., von Suchodoletz, H., Blanchard, H., Faust, D., Hambach, U. (2004): Reply to the comment by J.C. Carracedo et al. on ‘Geoarchaeological and chronometrical evidence...’. *Quaternary Science Reviews* 23, 2049–2052
- Zöller, L., Faust, D., von Suchodoletz, H. (2006): Pedostratigraphie des Quartärs auf Lanzarote. *Bayreuther Geowissenschaftliche Arbeiten* 27, 1–21.

## Tables

**Table 1**

Properties of studied sites on Lanzarote.

	<b>Guatiza</b>	<b>Femés</b>	<b>Teguisse</b>
latitude N	29°04′08″	28°55′32″	29°04′52″
longitude W	13°29′22″	13°45′19″	13°30′55″
altitude (m a.s.l.)	100	300	300
catchment area (km <sup>2</sup> )	10.1	5.07	3.8
valley bottom (% of catchment area)	16.1	18	35
relative elevation difference in the catchment area (m)	> 550	100-200	100
time of volcanic damming	170 ka <sup>1</sup>	1.0 Ma <sup>2</sup>	1.2 Ma <sup>3</sup>
volcanic damming complete?	no	yes	no
thickness of anthropogenic colluvial deposits (cm)	420	55	80

<sup>1</sup> consistent thermoluminescence and ESR data, Suchodoletz et al. (in preparation)

<sup>2</sup> Instituto Tecnológico y Geominero de España (2005), Coello et al. (1992)

<sup>3</sup> Instituto Tecnológico y Geominero de España (2005)

**Table 2**

Results of pedologic analyses and absolute clay contents. Furthermore, the detection of slickensides in the field as well as of anthophora bee nests are indicated and micromorphological features are interpreted (+ slight occurrence, ++ medium occurrence, +++ strong occurrence, - no occurrence) From these data, soil moisture relative to the lower precipitation limit of anthophora bees (200-300 mm/a) is derived for every layer (- < 200-300 mm/a; O 200-300 mm/a; +/++ somewhat/much more than 200-300 mm/a)

horizon	pH value	Na-saturation (%)	conductivity EC <sub>5</sub>	clay, pipette-analysis (mass-%, error 5%)	slickensides in the field	micromorphological features				Antophora bees	derived soil moisture
						vertic prop.	redox. Feat.	second. calcific.	clay illuv.		
<b>Femés</b>											
55 – 74	7.7	17.4	459	23	-						-
74 – 120	6.6	17.2	245	59	+	++	++	-	++		+
120 – 165	7.7	13.9	219	63	+					++ (100 m upslope)	O
165 - 200	7.6	17.3	227	63	++						++
200 – 240	7.6	14.2	236	78	+ / ++						++
240 – 270	7.7	15.0	250	76	+						+
270 – 315	7.8	12.6	288	27	-					++	O
315 – 365	7.7	18.8	289	41	+	-	-	++	-		+ / O
365 – 370					-					+	O
370 – 425	7.7	25.6	267	25	-						-
425 – 445					-					+	O
445 – 480	7.6	32.5	110.7	23	- / +						O / +
480 – 515	7.7	24.3	328	67	+	++	++	-	-		+
515 – 535	7.6	9.9	333	80	+ / ++	++	++	-	++		++
535 – 570	7.8	34.2	270		-					+	O
570 – 635	7.9	24.8	391	23	+						+
<b>Guatiza</b>											
420-450	7.8		260								
450-485	7.7		206			-	++	-	++	+	O / +

485-510	7.9		176.1							++	O
510-580	7.8		233			-	++	++	++		?
580-640	7.8		325								?
640-675	7.8		133								?
675-730	7.8		70			-	++	-	-	+	?
<b><i>Teguise</i></b>											
80-100	8.0	5.8	394		-					+	-/O
100-120	7.8	14.6	1365		+			++			-/O
120-142	8.0	14.1	1178		+						+
142-180	8.0	15.2	1494		+++	++	++		++		++
180-195	8.0	12.9	1423		++						++
195-220	8.0	12.2	1361		++	++	++		++		++
220-240	8.0	8.3	681		-					+	O
240-260	7.8	14.6	929		+++	++	++	++	+		++
260-290	7.9	16.4	1155		+++						++
290-350	7.9	17.0	1196		++	++	++				+/>++
350-388	8.2	13.5	1420		+					++	O
388-408					+						+
408-420	8.2	9.5	1032		+					++	O
420-475	7.8	18.3	914		+	++	++		++		++
475-510	8.0	18.6	2400		-					+	O
510-550	8.1	13.0	895		-					+	O
550-590	7.8	13.4	132.8		-		++		+		
590-635	8.0	12.4	377		-						?

**Table 3**

Allophane analyses from Femés.

Al<sub>o</sub> = oxalate soluble Al, Si<sub>o</sub> = oxalate soluble Si, Al<sub>d</sub> = dithionite soluble Al, Si<sub>d</sub> = dithionite soluble Si.

depth (cm)	Al <sub>o</sub> (mg/kg)	Si <sub>o</sub> (mg/kg)	Al <sub>d</sub> (mg/kg)	Si <sub>d</sub> (mg/kg)
65	1343	231	1168	101
205	1463	< 180	1134	< 90
525	1394	< 180	972	< 90

**Table 4:**

Micromorphological features of investigated horizons in all profiles.

<sup>a</sup> u = undifferentiated, ms = mosaic speckled, ss = stipple speckled, gs = granostriated, ps = porostriated, s = striated, c = crystallitic.

<sup>b</sup> t = typical, c = concentric, a = aggregate; hc = hypocoating, cc = clay coating.

<sup>c</sup> d = dusty, li = limpid, c-s = clay-silt, f = fragment; li-f = limpid fragment.

<sup>d</sup> mhc = micritic hypocoating, mn = micritic nodule, sp = sparite, prc = primary carbonate

<sup>e</sup> sp = spongy, sb = subangular blocky, ab = angular blocky, pl = platy, gr = granular, ma = massive

horizon depth (cm)	groundmass							pedofeatures											microstructure <sup>e</sup>								
	micromass							translocation features																			
	b-fabric <sup>a</sup>							redoximorphic <sup>b</sup>				clay coating <sup>c</sup>					carbonate <sup>d</sup>										
	u	ms	ss	gs	ps	s	c	t	c	a	hc	d	l	c-s	f	li-f	mhc	mn	sp	prc	sp	sb	ab	pl	gr	ma	
<b>Femés</b>																											
108-113				X	X	X			X	X			X					X	X						(X)		
358-363							X							X			X									X	
498-503			X	X	X	X				X								X							X	X	
535-545					X			X		X	X		X		X										X	X	
<b>Teguisse</b>																											
100-120			X	X	(X)	X		X									X	X						X	X		
142-180		X	X	X	X			X		X			X		X			X	X	X				X	(X)	X	
195-220		X	X	X	X			X		X	X		X	X		X				(X)					X		X
240-260		X	X	X	X	X		X		X	X		(X)				X	X	X					X	X		
290-350		X	X	X	X	X		X		X	X				(X)									X	X	(X)	
420-475		X	X	(X)	X	X		X		X			X											X	X	X	
550-590			X	(X)						X	(X)		X		(X)									(X)	X	(X)	
<b>Guatiza</b>																											
450-485		X		(X)				X		X			X	X		X			X						X		X
510-580			X	(X)					X	X	X		X	X		X		X	X					(X)	X		X
675-730		X		(X)			X			X	X		X		X									X		X	

x = frequent occurrence, (x) = subordinate occurrence

## Figures

**Figure 1**

Location of Lanzarote and studied sites.

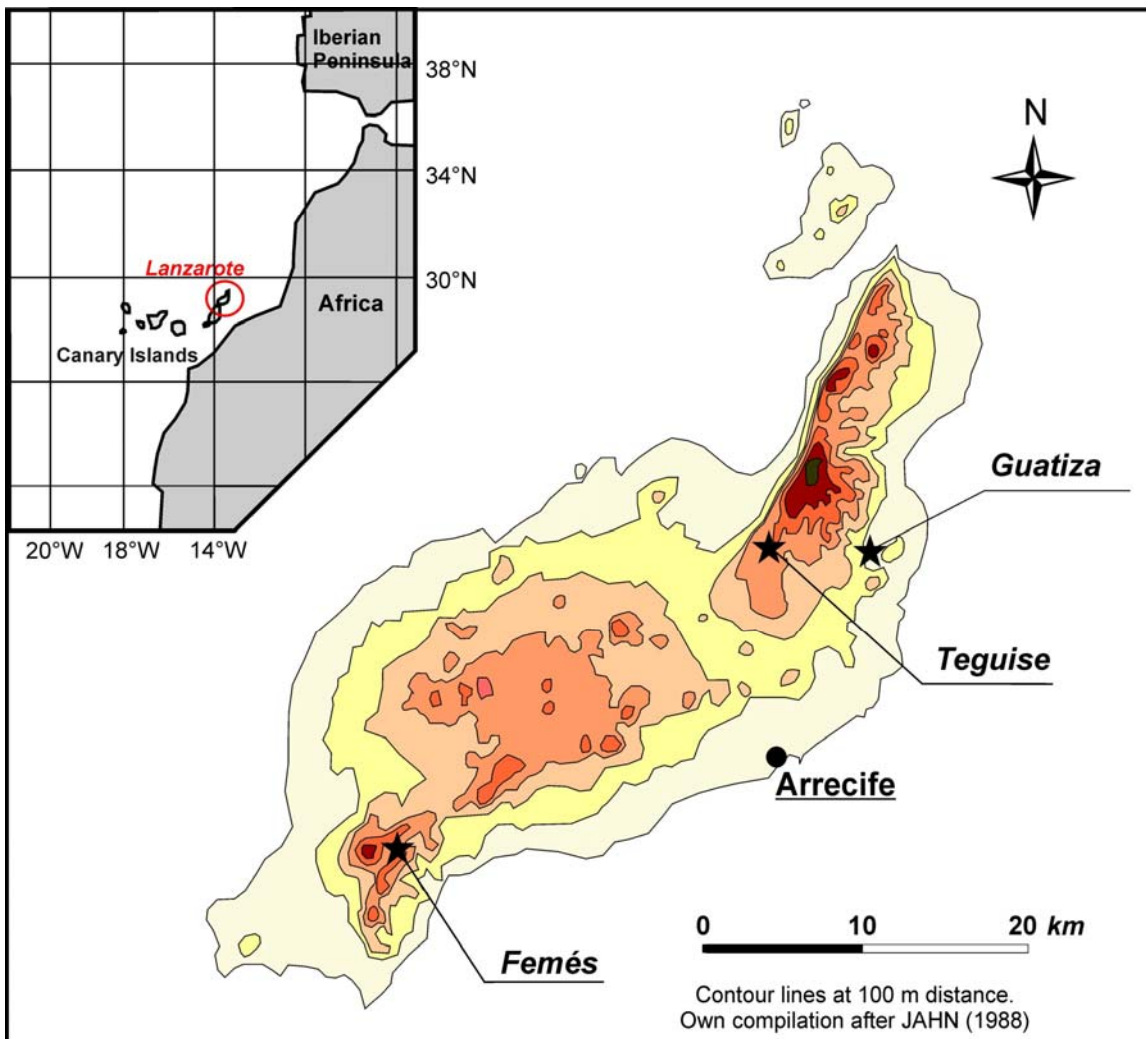


**Figure 2**  
Investigated profiles with luminescence ages.

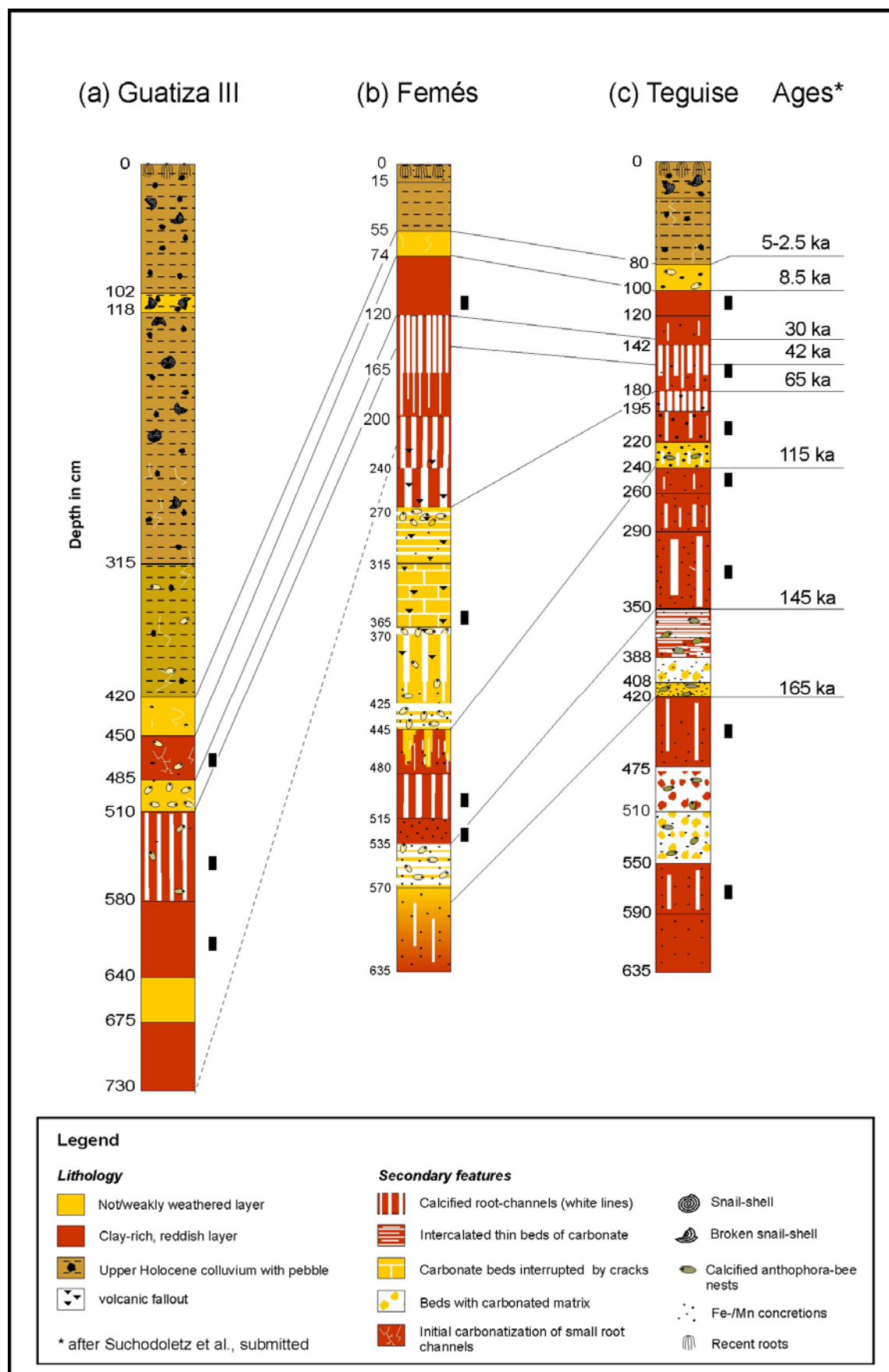


**Figure 3**

Dark-brown aggregates inclosing smaller grains in the sieved and HCl-treated fraction  $< 63 \mu\text{m}$  from a reddish clay horizon in Femés (230 cm). Two examples are marked with arrows.

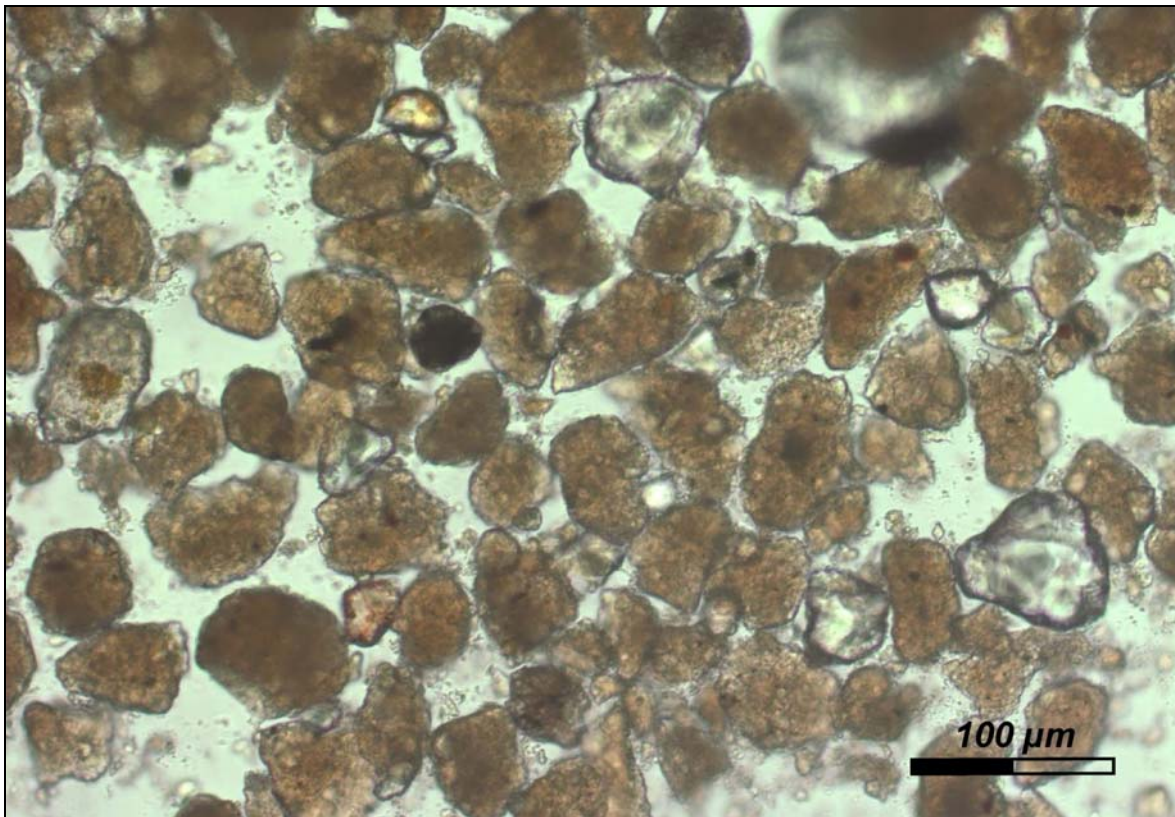


**Figure 4**

Comparison of relative clay contents derived by laser analysis with absolute clay contents derived by pipette analysis from the profile of Fêmes.

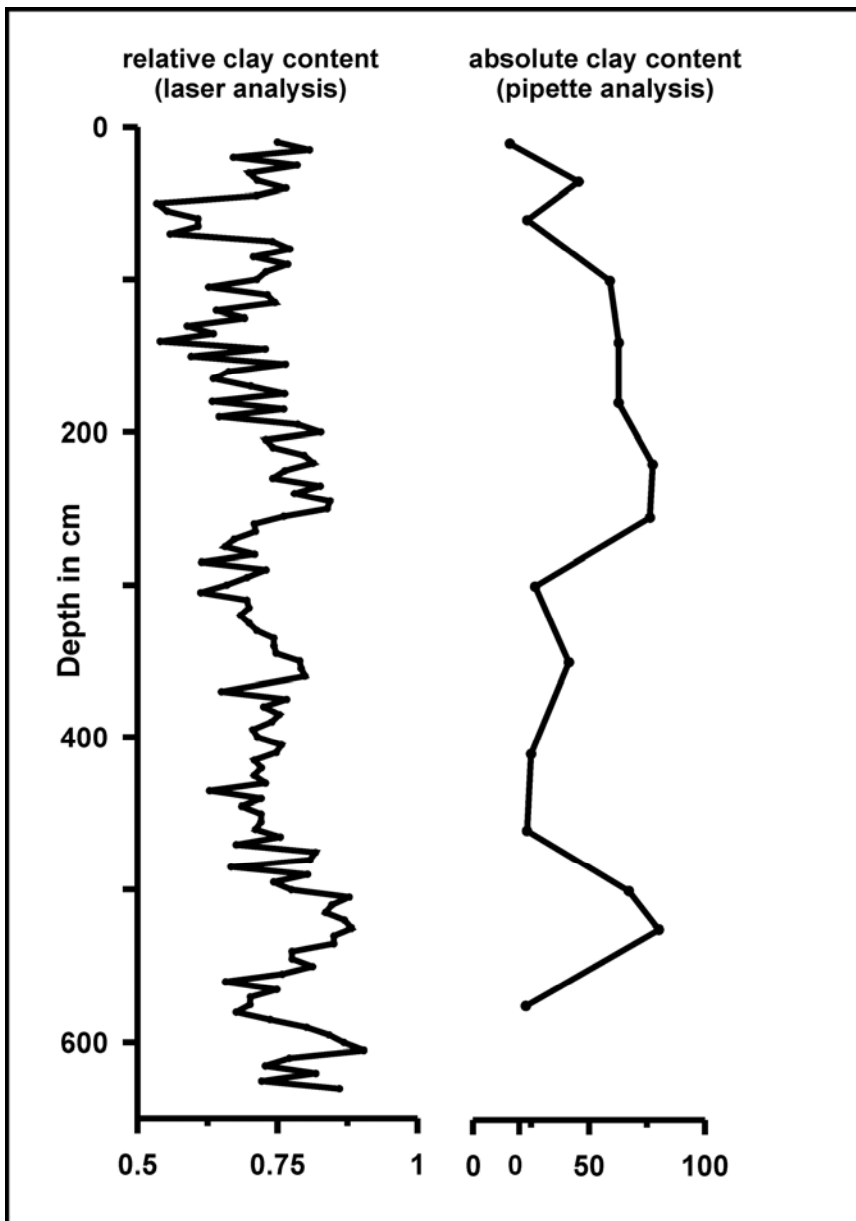


**Figure 5**

Proxies from the vegas of Lanzarote: a) initial magnetic susceptibility ( $\kappa$ ,  $10^{-6}$  SI-units), b) isothermal remanent magnetisation (IRM,  $A\ m^{-1}$ ), c) frequency dependent susceptibility ( $\kappa_{fd}$ , %), d) IRM/ $\kappa$  ( $kA\ m^{-1}$ ), e) relative clay content (arbitrary units), f) relative bulk illite content (arbitrary units), g) relative bulk kaolinite content (arbitrary units), h) absolute bulk quartz content (%), i) carbonate in matrix (%). Shaded layers indicate soil sediment layers and upper hatched layers anthropogenic colluvial deposits.

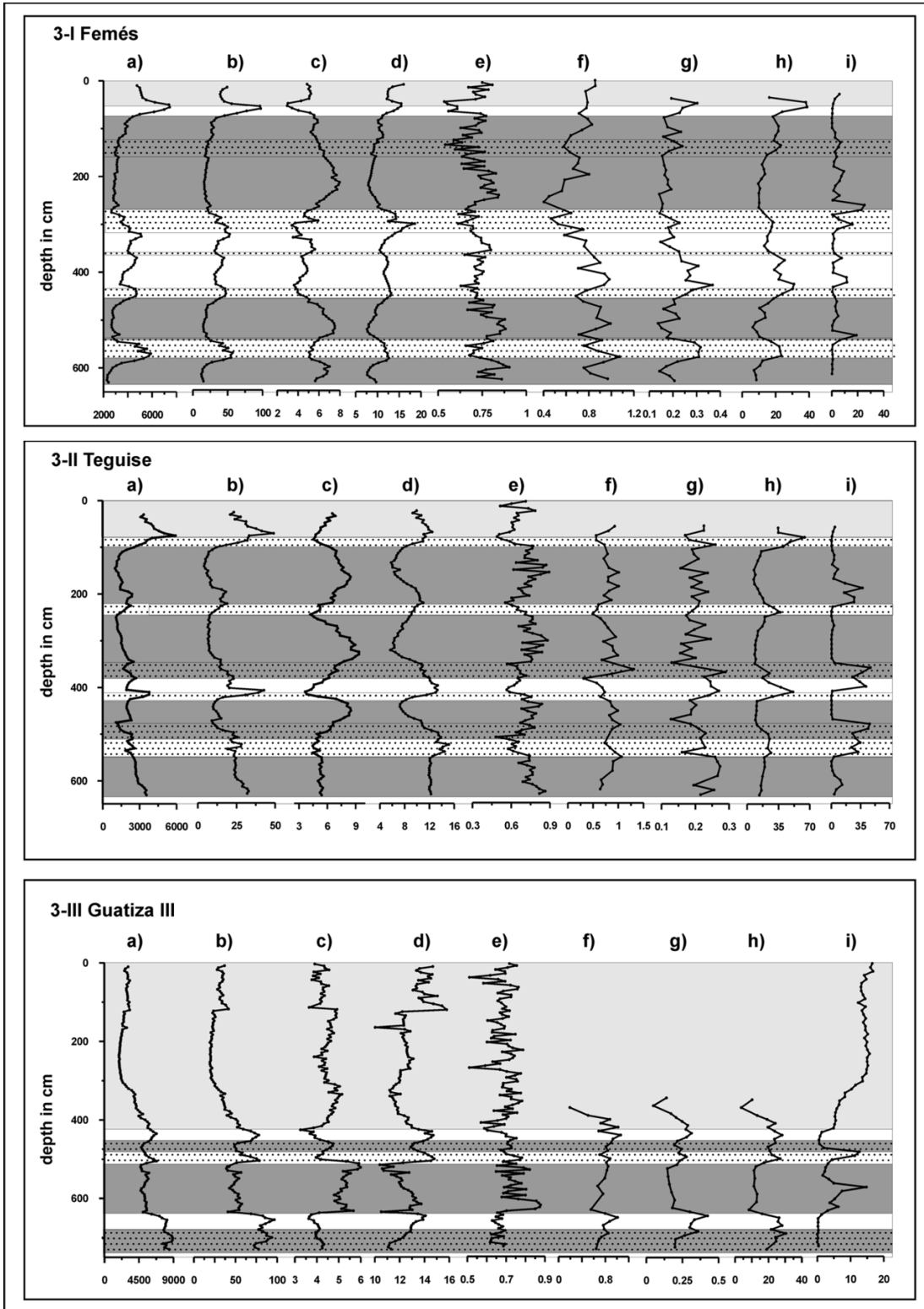


**Figure 6**

X-ray diffractograms from the investigated clay samples < 2  $\mu\text{m}$  from Femés. The peaks of kaolinite and illite/muscovite are clearly recognizable, whereas that of smectite is absent or very faint. Black lines indicate graphs of untreated pulver aliquots, grey lines show measurements after a treatment of the material with glycole.

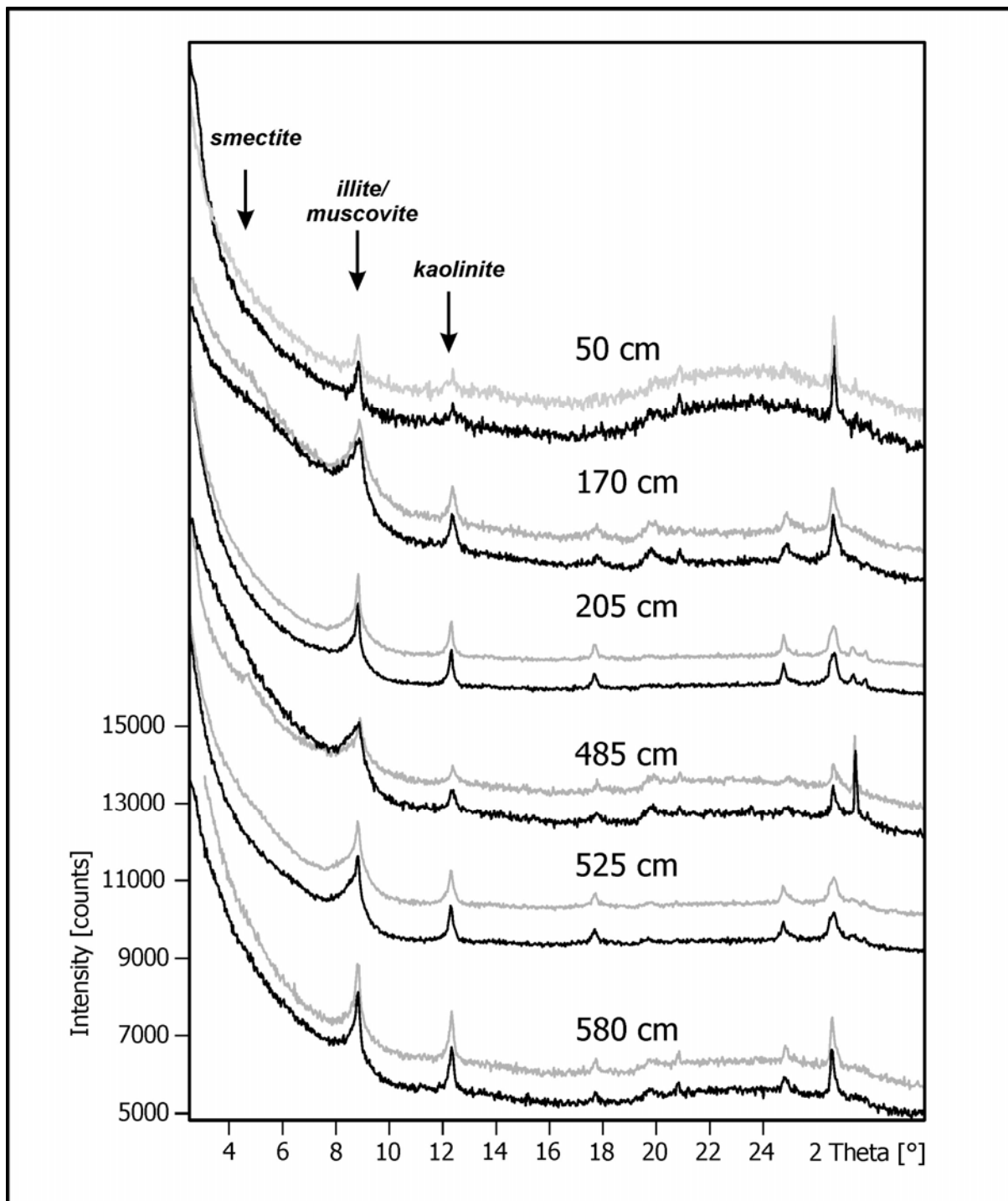


**Figure 7**

a) Cross-plot of IRM acquired at fields of 2 T to low field magnetic volume susceptibility ( $\kappa$ ). Both parameters are strongly concentration dependent. The strong linear correlation proves the dependency of the magnetic susceptibility signal on remanence carrying – probably ferromagnetic – minerals. The intersections of the linear fits with the susceptibility axis clearly indicate the para- and superparamagnetic contributions to the magnetic susceptibility signal. Note the distinct grouping of the individual sites. For Guatiza only the data from the non-anthropogenic interval are plotted.

b) Cross-plot of the frequency dependent susceptibility ( $\kappa_{fd}$ ) to the IRM/ $\kappa$  ratio. Both parameters are generally mineral and/or grain size dependent, but absolutely independent from variations in concentration. The obvious anticorrelation indicates the overall control of the parameters by a non-remanence carrying but highly susceptible mineral fraction. This fraction is most probably formed by superparamagnetic particles derived from weathering of the primarily detrital ferrimagnetic minerals. Note the distinct grouping of the individual sites. The obvious stronger pedogenetic overprint in Teguisse compared to the other profiles is also visible in the field and can be explained by enhanced humidity due to the close proximity of this profile to the sea. For Guatiza only the data from the non-anthropogenic interval are plotted.

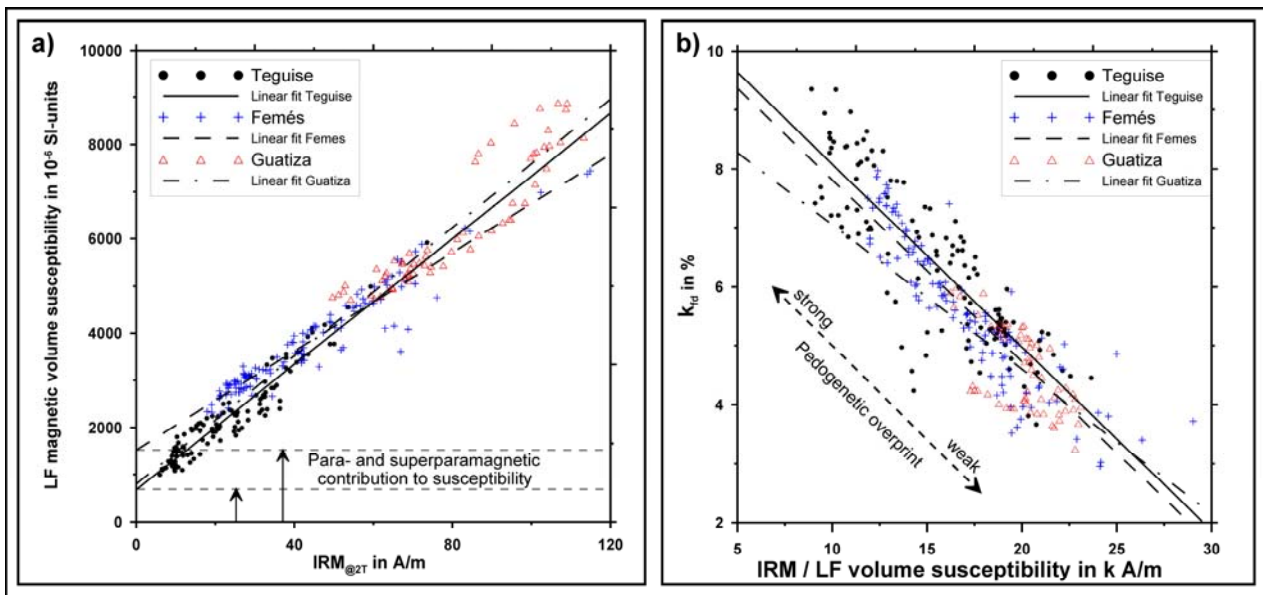


**Figure 8**

Micromorphological features.

- a) Ferruginous hypocoating on groundmass (white arrows) and typical ferruginous nodules. Note the granostriated b-fabric resulting from physical stress — Femés, 108–113 cm, crossed polariser.
- b) Fragment of clay coating (black arrow) within non calcareous ped. Grey areas indicate secondary calcification by micritic carbonate — Femés, 358–363 cm, one polariser.
- c) Small yellow brown clay coatings (yellow arrows). Porostriated b-fabric and pressure faces (blue arrows) indicating physical stress — Femés, 535–545 cm, crossed polariser.
- d) Small yellow brown clay coatings (yellow arrows) and pressure faces (blue arrows). Pressure faces are not distinguishable from groundmass using one polariser. Fragment of clay coating within ped (white arrow) — Femés, 535–545 cm, same as 8c, but with one polariser.
- e) Micritic hypocoatings around channels and pressure faces (yellowish striae). Note the ferruginous nodule without granostriation in the upper right corner— Teguise, 240–260 cm, crossed polariser.
- f) Weathered volcanic glass (blue arrows) with granostriated b-fabric. Clay domains within the glass indicate weathering to clay—Teguise, 240–260 cm, crossed polariser.
- g) Numerous grains of glauconite (e.g. in the centre) indicate the influence of marine sediments — Teguisse, 550–590 cm.

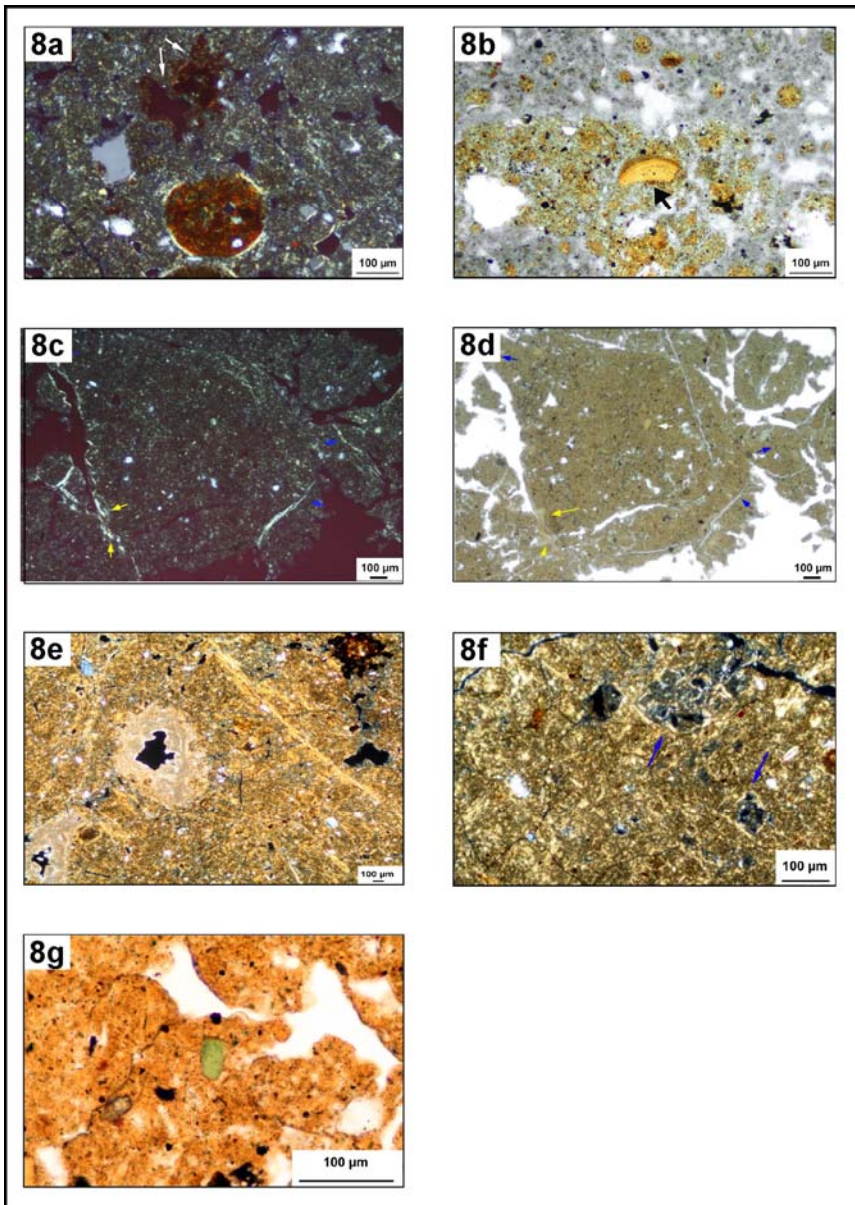


**Figure 9**

Strong shrinking cracks developed on the surface of recently formed colluvial deposits in Guatiza.



**Figure 10**

Compilation of profiles, ages and palaeoenvironmental proxies: a) vertic properties derived from field and micromorphological analysis, merged with the occurrence of ground-nesting anthophora-bees (arbitrary scale), b) relative clay content (arbitrary scale), c) frequency dependent magnetic susceptibility (%). Shaded sections indicate more arid periods, hatched areas anthropogenically triggered colluvia. Due to the lack of palaeoenvironmental significance of these layers, vertic properties were not investigated in these colluvia. Ages and Marine Isotope Stages (MIS) are indicated on the right side.

